Towards a Carbon Nanotube Antibody Sensor

by

Peter Bojö

B.S. Biological Engineering
MIT 2010

SUBMITTED TO THE DEPARTMENT OF BIOLOGICAL ENGINEERING IN PARTIAL FULFILLMENT OF THE REQUIREMENTS FOR THE DEGREE OF

MASTER OF ENGINEERING IN BIOLOGICAL ENGINEERING
AT THE
MASSACUSETTS INSTITUTE OF TECHNOLOGY

SEPTEMBER 2011
[February 2012]

Signature of Author: _____
Department of Biological Engineering
September 4, 2011

Certified by: _____
Michael Strano
Associate Professor of Chemical Engineering
Thesis Supervisor

Certified by: _____
Dane Wittrup
Professor of Chemical and Biological Engineering
Biological Engineering Reader

Accepted by: _____
Forest White
Associate Professor of Biological Engineering
Co–director of the MEBE program

1. Abstract

This work investigated single-walled carbon nanotube (SWNT)/polymer-protein A complexes for optically reporting antibody concentration via a change in near infrared fluorescent emission after antibody binding. SWNT have potential as biosensors because of extraordinary sensitivity, lack of photobleaching, and optical activity in a near-infrared window. A SWNT sensor could provide label-free measurements of antibody concentration in a continuous fashion, which may aid selection of production strains. Protein A itself, dextran, poly vinyl alcohol, DNA sequences, and chitosan were used as polymers for wrapping SWNT. Nonspecific binding to solution-phase constructs was found to be a major problem with these approaches. Chitosan hydrogels encapsulating SWNT also show nonspecific responses.

Table of Contents

2. Acknowledgments

I have benefited from much input and encouragement throughout my work on this project. Above all, Prof. Strano has guided me through the process of which questions to ask when my focus might otherwise have strayed.

In the lab, Jong-Ho and Nigel are to thank for inventing the chitosan chip technique and helping me learn it. Arde and Jingqing were always very happy to help with getting me familiarized with new equipment and taking care of miscellaneous details. Selda and Fatih were very helpful with single molecule experiments. Finally, although I did not do any work with them, Joel, Rishab, Steven, Andrew, and Tom were friendly people to be around while working. I will miss being around everyone in the lab.

My undergraduate research experiences under Qiaobing Xu and Chris Pritchard in the Langer lab were a key part of my MIT experience, and they convinced me that taking on my own research project would be an interesting next step. I have gained some of their passion for science.

My friends in the Auburn street apartment were always around to recharge with some Fifa, MOM, or tennis.

Finally, I'd like to thank my parents for their patience in listening to the ups and downs of research, and their cheerful and logical advice along the way.

3. Introduction

The goal of my research was to design and synthesize a protein A-polymer/ single-walled carbon nanotube (SWNT) complex to optically report antibody binding via a change in near infrared fluorescent emission. This would allow for a SWNT based sensor to rapidly report antibody concentrations, potentially in real-time.

3.1 Nanotube sensors

SWNT are cyclindrical structures composed entirely of sp^2 hybridized carbon atoms. They were discovered in 1991 by Sumio Iijima. Typical nanotubes have a diameter on the order of 1nm and have been grown as long as 18.5cm(Wang X 2009). Nanotubes differ in their chiral angle, a set of two numbers (n,m), which defines how a flat sheet of graphene should be rolled up in order to create the nanotube. There are zigzag (n=0,m=0), chiral (m is not 0 or n), and armchair (m=n) nanotubes. Armchair nanotubes are metallic while the other species are semiconducting.

SWNT have been attracting significant attention in research because of many advantageous optical, electrical, and mechanical characteristics. The one-dimensional electronic structure of nanotubes creates clear emission peaks in the near infrared (900-1400nm), which can be altered by interaction of analytes with the nanotube surface (Satishkumar 2007; Zhang, Boghossian et al. 2011), forming the conceptual basis for a sensor. The dielectric constant of the media surrounding the nanotube is a key variable influencing the optical transition energy (Strano 2007), but the local dielectric constant for complicated solutions is not apparent. Nanotube sensors have the advantages that no photobleaching threshold has been reported (Saito 1998; Daniel A. Heller 2005) and adsorption of single-molecules to the nanotube sidewall has been reported (Laurent Cognet 2007; Anni J. Siitonen 2010; Hong Jin 2010). Additionally, the near infrared wavelengths used for excitation and monitored for emission fall within the near infrared window in biological systems, where light penetrates tissue relatively well, making the use of the sensor with a cell culture system a definite possibility (L. R. Hirsch 2003). This work focused predominantly on probing nanotubes through photoluminescence, where a photon excites an electron into the valence band, creating an electron-hole pair or exciton. The exciton generally undergoes nonradiative decay, but sometimes, generally around 1% of the

time, the electron recombines with the hole and a photon is emitted (Sang-Yong Ju 2009). This process only occurs in semiconducting nanotubes.

The polymer or protein serves the role of keeping the system colloidally stable. SWNT powder consists of many bundled SWNT held together by strong van der Waals forces, and while the sonication procedure separates the nanotubes, the polymer or protein attaches to the newly dispersed nanotubes via hydrophobic interactions(Faiella G 2009).

SWNTs are being investigated as materials for reinforced composites due to their extremely high Young modulus and tensile strength. For example, some of the first commercial applications of SWNT include epoxys with carbon nanotubes which boast increased strength (Amroy 2011). SWNT are also being investigated as promising candidates for miniaturized electronics because metallic nanotubes behave as excellent conductors which generate much less heat, even when running high currents, because of their ballistic mode of conduction (Ando 2009; ScienceDaily 2009). These mechanical and electrical characteristics are not exploited in this work.

The biocompatibility of SWNT is a growing area of research. Cytotoxicity has been shown *in vitro.* For example, about 30% of alveolar macrophages died upon exposure to 11.30 $\mu g/cm^2$ of SWNT dispersed via ultrasonication without a surfactant (Guang Jia 2009). *In vivo m*ice show dose-dependent oxidative stress, acute inflammation, and fibrosis after pharyngeal aspiration or exposure to aerosolized as-produced HiPco SWNT. Various measures of inflammation, such as the numbers of polymorphonuclear leukocytes and alveolar macrophages, are significant at exposure levels of $5\mu g$/mouse or 5 mg/m^3 for 5 h/day for 4 days (A. A. Shvedova 2008). Interestingly, pristine SWNT have been shown to be biodegraded by the neutrophil enzyme human myeloperoxidase, creating shorter non-inflammatory nanotubes (Valerian E. Kagan 2010). While all of these studies suggest that SWNT biocompatibility merits further research, since the biological applications of SWNT, for either sensing or drug delivery, will use SWNT suspended in polymers, toxicity studies with the specific SWNT/polymer system will need to be performed. For example, despite demonstrated toxicity of pristine nanotubes, the Dai lab showed that PEG suspended SWNT show no toxic side effects after IV injection and was cleared almost completely after 2 months (Zhuang Liu 2008).

The Strano group has developed many SWNT based fluorescent sensors, including sensors for the detection of glucose (Paul W. Barone 2009), Nitric oxide(Zhang, Boghossian et al. 2011), protein-protein interactions(Jin-Ho Ahn 2011), hydrogen peroxide(Hong Jin 2010), and ATP(Jong-Ho Kim 2010). The expertise accumulated from the development of these successful systems provided a logical opportunity for development of protein A based antibody sensor. All of these sensors are based on changes in photoluminescence.

Due to the relatively recent discovery of nanotubes in 1991, nanotubes are not yet a standardized commodity. There are several nanotube vendors, who all supply slightly different nanotubes. For example, SouthWest NanoTechnologies' CoMoCat nanotubes are produced by flowing pure CO at a total pressure between 1 and 10 atm and at a temperature of 700-950ºC over a Cobalt and molybdenum catalyst. There is a hydrogen reduction step after this. Samples contain over 50% (6,5) nanotubes, as well as a significant number of (7,6) nanotubes (NanoTechnologies 2011). Nano-C nanotubes are produced by an unknown method with multiple combustion gases, a catalyst, and a purification step (Nano-C 2011). Nano-C samples contain many chiralities.

3.2 Antibodies

Antibodies are an extraordinarily versatile class of molecules with which the immune system combats perpetually evolving threats. Antibodies complexed with antigen trigger complement activation by binding to C1q, which eventually leads to the formation of membrane attack complexes. Complexed antibodies will also bind to Fc receptors on leukocytes, which will trigger different cytotoxic effector functions, such as release of lysosomal enzymes (Hamilton 2001).

Antibodies have 4-18% carbohydrate and are made up of two identical heavy chains, each ~50kDA, and two identical light chains, each ~25kDA, for a total weight of about 150kDA. The heavy and light chains have disulfide bridges between them. Antibodies are split into IgM, IgD, IgG, IgE, and IgA classes depending on substantial differences in their heavy chains. The primary sequences of IgG heavy chains are over 95% identical. The critical variation is in the

hypervariable loops, made up of residues from the heavy and light chains, which creates the diverse specificity of antibody targets. There are three hypervariable regions present in each of the two IgG antigen binding arms. The hinge region is also a site of variability. IgG1 is the most highly concentrated IgG and is generally present at around 10mg/mL in adults. The structure of an IgG1 antibody is seen in Figure 1. Both the antigen binding regions (Fab regions) and the constant 'crystallizable' region (Fc region) are shown (Hamilton 2001).

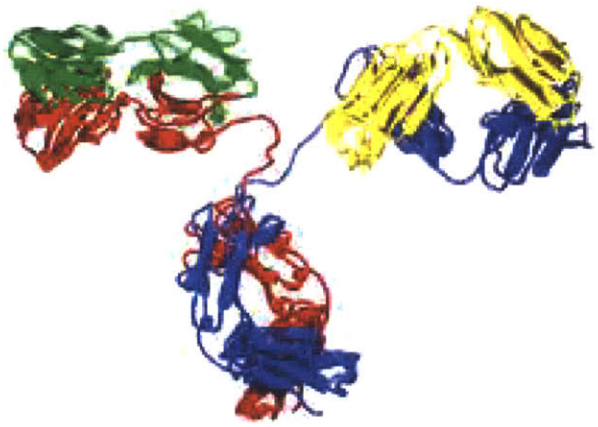

Figure 1: A ribbon diagram of an IgG2 anti-canine lymphoma monoclonal antibody. The heavy chains are shown in red and blue. The light chains are shown in green and yellow. The two bottom bundles of the red and blue chains together constitute the Fc region. The rest of the protein constitutes the Fab region. The PDB code is 1IGT.

Monoclonal antibodies had aggregate global sales of $38 billion in 2009. The top selling monoclonal antibodies include cancer targeting antibodies, such as Herceptin and Avastin, and anti-tumor necrosis alpha antibodies, such as Enbrel and Remicade, which are used for treatment of rheumatoid arthritis and Crohn's disease. The total market for protein based therapeutics is expected to show an annual growth rate between 7-15% in the next several years(Walsh 2010).

Manufacture of monoclonal antibodies was first made possible by hybridoma technology, which created immortalized antibody producing cells by fusing a B cell with a myeloma cell. There are now many manufacturing systems, including CHO cells, yeast cells, and even efforts to create transgenic goats (Kling 2009).

Global antibody sales are impressive, and so are the costs associated with producing antibodies. Companies advancing antibodies are required by the FDA to have a Master Cell

Bank (MCB), which is a collection of cells which are meant to provide an identical starting point for production runs and certified to be free from contamination. For any company developing a monoclonal antibody there is inevitably a race to get the antibody onto the market as quickly as possible, in order to maximize the revenues achieved while patent protection still prevents generic companies from selling an identical product. As an aside, patent expiration may not be the end of a market monopoly for the innovating company when it comes to antibodies because no antibody biosimilars have been approved, and there is regulatory uncertainty as to whether they will be allowed. Different glycoforms, disulfide pairing, deamidation, and cyclization of N-terminal glutamine residues make antibody manufacturing a particularly tricky biosimilar manufacturing task (Initiative 2010). Regardless, profit is being lost if product launch is delayed. The incentive to get the antibody to market quickly may cause companies to begin testing their antibodies with suboptimal MCB titers. Companies can work on obtaining a more highly productive MCB in parallel with clinical trials, but additional animal and human testing may be required to prove that the end product is analytically equivalent (Fenno 2007). A potential issue is a change in glycosolation, which could trigger an immune response or alter the antibody mediated cytoxicity (Thommes 2010). There are contract manufacturing organizations which utilize proprietary techniques in order to boost antibody titer. For example, Catalent offers 'GPEx technology' which consists of inserting genes coding for the protein product at multiple genomic locations by RNA retroviruses which cannot replicate, but carry the protein product genes, reverse transcriptase, and integrase (Catalent 2011).

The quest to establish a stable master cell bank with a high titer is a critical determinant of product cost. A survey of the economics of monoclonal antibody production called titer 'the overriding cost driver in producing monoclonal antibodies' (Farid 2007).

In order to boost cell productivity there has been a research focus on increasing gene copy number and transcriptional rate. Specific efforts include identifying stronger promoters, site specific integration of DNA, including DNA that prevents heterochromatin repression, use of Internal Ribosome Entry Sites, and improving folding kinetics through manipulation of BiP, PDI, and other chaperones (James 2009). Regardless of the particular method of creating a pool of

antibody producing cells with a range of productivity, some strategy must be employed to identify those that are stable and highly productive cells.

Current methods for selecting highly productive antibody producing cells are reviewed by Browne et al. and Shukla et al. (Al-Rubeai 2007; Thommes 2010). They include Limited Dilution Cloning (LDC), Fluorescence activated cell sorting (FACS), gel microdrop technology, and automated cell selection systems. In LDC single cells are seeded into well plates and then ELISA, or similar techniques, is used. It is slow and widely used. FACS is high throughput but relies on the ability to fluorescently tag the produced antibody or a molecule that is presumed to be linked to the amount of antibody production. For example, GFP can be co-expressed with the heavy and/or light chains, a surface protein can be co-expressed with the antibody and later detected with a fluorescent antibody, or fluorescently labeled methotrexate can be added to cells transfected with a vector which contains dihydrofolate reductase (binding of the methotrexate to the dihydrofolate reductase acts as a reporting scheme for how many copies of the vector were integrated into the host genome). The reporting gene is often driven by a weak promoter, whereas light and heavy chain expression is driven by a strong promoter such as the cytomegalovirus promoter. These FACS based methods are a drastic improvement over LDC, but fluorescence may not always correspond to short or long-term productivity (Al-Rubeai 2007; Warren Pilbrough 2009; Ye 2010). Gel microdrops are a technique which immobilizes the secreted antibodies within a polymer gel and then relies on a series of biotin, avidin, and antibody interactions to create fluorescence proportional to the immobilized antibody. Automated cell selection systems use a fluorescently labeled antibody to quantify the amount of antibody being secreted by a spot of immobilized cells and then select productive spots by physically picking them (ClonePix, Cellcollector) or by destroying only the less productive spots with a laser (LEAP). Both gel microdrops and automated cell selection systems require a detection antibody with a fluorescent label to be designed against the antibody being produced.

3.3 Rationale for a SWNT-based Antibody Sensor

A SWNT based sensor would have a number of advantages over these technologies: first, no labeling of the target antibody or cell producing that antibody is required; second, it matches or exceeds the throughput of the above technologies; third, the productivity of cells can be monitored almost continuously. These advantages are particularly important in cases where raising an antibody against the secreted antibody is difficult or if the long-term stability of expression can be predicted by continuous time measurements.

The latter possibility is a particularly intriguing potential advantage of a sensor which can probe antibody concentrations at much smaller timescales than is currently possible. Such measurements might be able to monitor bursts of productivity and relate this to unstable productivity. In other words, better time resolution of antibody secretion by single cells may help to identify cells which appear to be high producers only due to bursts caused by temporary promoter activation versus genuine high producers which benefit from a favorable genomic change as a result of mutation or vector integration. The snapshots of integrated productivity provided by LDC, FACS, gel microdrops, and automated cell selection systems do not reveal any of the potentially important details related to how cells respond to growth and environmental conditions (Kerry Routenberg Love 2010). Monitoring changes in secretion due to changing conditions could help optimize fermentations. Pilbrough and co-workers showed that there is very high *intraclonal* variation in antibody expression in CHO cells (Warren Pilbrough 2009), which makes it more critical that genuine high producers can be selected early in the manufacturing process.

There are other label-free technologies which have the potential to fill the same need as a SWNT-based sensor. Label free protein detection is reviewed by Ray et al. (Sandipan Ray 2010). One technique is a nanohole array, which relies on monitoring the refractive index of the medium on a metal surface through extraordinary optical transmission, which is light transmission through a periodic array of subwavelength holes which is orders of magnitude higher than is classically predicted. Each detection spot is ~10μm^2, theoretically allowing tens of thousands of spots on a single chip, and was used to detect anti-GST antibodies with a CCD camera after immobilization of glutathione S-transferase (Jin Ji 2008). Oblique-incidence

optical reflectivity difference is able to distinguish binding events based on changes in the ratio of the transverse magnetic and electric modes, and was used to image goat anti-mouse antibody and other protein-protein interactions on a 2,760 spot microarray (Y.Y. Fei 2008). Enthalpy arrays, which are nanocalorimeters which electrostatically merge 250nL and then measure temperature change, have the potential to be miniaturized but were reported to have a K_d detection limit of only 5μM (Recht MI 2008). Silicon nanowire field effect transistors were shown by the Lieber group to be capable of detecting ATP binding to the immobilized protein Abl, but a high-throughput system has not been reported by the group (Wayne U. Wang 2005). Microcantilevers, where binding of molecules to an immobilized target causes a change in the resonant frequency of the lever, and interference based techniques, where an optical phase difference due to mass change is detected, are also reviewed (Sandipan Ray 2010).

In summary, a SWNT based sensor provides an attractive platform for label-free, high-throughput, and continuous testing of cell productivity, which may help to address confounding intraclonal expression variation. We envision that the sensor could be incorporated into microspheres encapsulating clonal populations of cells or embedded in a film, reporting local antibody concentrations and allowing high-producing cell lines to be identified. Such a sensor would need to be complemented by assays validating the functionality of the antibody, since protein A will interact mostly with the heavy chain, regardless of the presence of the light chain.

3.4 Plan for Making a Protein A Sensor

In order to make a sensor specific to antibodies, we choose to use protein A, because it binds specifically to a broad spectrum of antibodies. The protein has cleverly evolved in *Staphylococcus* to sit on the outside of the bacteria and prevent phagocytosis by binding the constant region (Fc region) of antibodies (Phillip Peterson 1977). Normally, receptors on the cells of the immune system will bind to exposed Fc regions of antibodies which have recognized a foreign antigen and bound to it, but Protein A effectively hides the Fc region from the immune cells and thereby slows opsonization. Protein A has a signal sequence directing it to the outside of the cell, five similar antibody binding domains, and a cell wall anchoring sequence. The antibody binding domains contain three alpha helices each and are

approximately 60 amino acids long(Hober S 2007). In addition to high affinity for the Fc regions of many antibody isotypes, some affinity for Fab regions has been described(Enrico A Sturaa 2001).

We took two conceptually different approaches to creating this SWNT and protein A based conjugate capable of signal transduction. In general, the approaches comprised of either 1) wrapping the SWNT non-covalently with a polymer and then covalently attaching Protein A to the polymer or 2) suspending the SWNT directly with Protein A. The polymers used were dextran functionalized with phenoxyl groups, poly vinyl alcohol, DNA sequences, and chitosan. An idealized sensor is depicted in Figure 2.

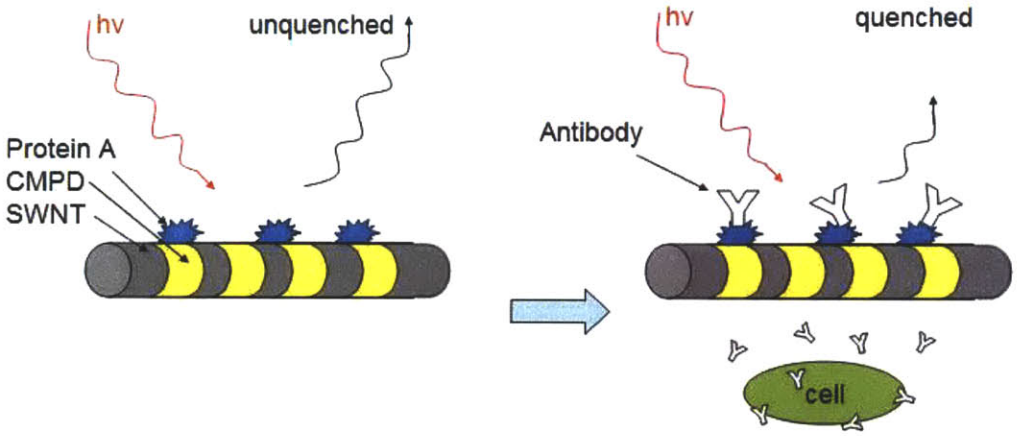

Figure 2: Idealized protein A-polymer/SWNT sensor. Near infrared light is used to show to what degree antibodies are bound to protein A on the sensor surface. In this case the specific polymer is labeled as CMPD. The SWNT is not to scale with the proteins.

A sample SWNT/polymer-Protein A synthesis scheme is included in Figure 3. Excitation-emission profiles of the SWNT/polymer-Protein A complexes were measured to check for a concentration-dependent response to IgG. The antibodies were selected from chromatographic studies of protein A which showed which antibodies protein A has affinity for, which is summarized in Figure 4 (Hober S 2007). A spectral deconvolution program was used to assess the contribution of each species of nanotube to the excitation-emission spectrum. Typical concentrations of antibody in assays were in the 0-1000nM range. If binding is due to protein A and antibody interaction, we expect to see a characteristic sigmoidal signal versus IgG

concentration response of the SWNT/polymer-Protein A complex, but not observe that response with the SWNT/polymer complex which lacks Protein A. Effective sensor K_d can be compared to native protein A-IgG K_d, which indicates to what extent a lowered protein A affinity, due to surface immobilization on the SWNT, and imperfect quenching upon IgG binding, is present.

It is important to note that most therapeutic antibodies are human IgG1 antibodies, so they will be amenable to binding protein A attached to a nanotube (Xiaoling Wang 2009; Carter 2010). In fact, protein A purification is a standard purification technique used by drug companies (Thommes 2010).

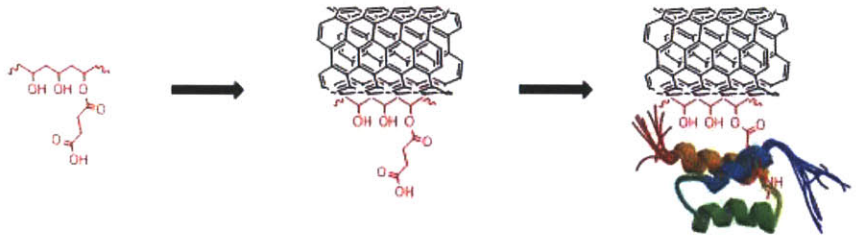

Figure 3: Overview of synthesis of SWNT/cPVA-Protein A complex. The first step is a dialysis of SC/SWNT with cPVA. The second step is EDC/NHS coupling of the cPVA to the protein A, which is represented by the protein ribbon diagram.

Species	Subclasses	Protein A
Human	IgG1	++
	IgG2	++
	IgG3	–
	IgG4	++
	IgA	Variable
	IgD	–
	IgM	Variable
Rabbit	No distinction	++
Guinea pig	IgG1	++
	IgG2	++
Bovine		+
Mouse	IgG1	+
	IgG2a	++
	IgG2b	+
	IgG3	+
	IgGM	Variable
Chicken	IgY	–

Figure 4. Staphylococcus Protein A affinity for Immunoglobulin classes. Adapted from Hober et al. Strong binding is ++, medium binding is +, negligible binding is -.

4. Materials and Methods

Dialysis of SC/SWNT with Protein A: 3mL of 2wt% SC/SWNT was mixed with Protein A for a final concentration of 300μg/mL Protein A. This solution was added to a dialysis cartridge (Pearson). The cartridge was placed in 2L of stirred PBS for 24hr. If necessary, the pH of the 2L solution was adjusted using diluted HCl or NaOH solutions. The 2L solution was changed at least once during the procedure.

Aggregated nanotubes were filtered out by centrifuging the final solution for 5 hours at 16000g in 1.5mL microcentrifuge tubes. Care was taken to remove only the supernatant, leaving a little liquid so the pellet was not disturbed. Free protein A was filtered out using 100kDA Amicon filters at 4000 RPM for 2 minutes.

Synthesis of cPVA: 6g of PVA powder was added into 200mL of NMP solution in a round bottom flask. The temperature was raised to 80°C with vigorous stirring to dissolve the PVA completely. 0.525g of DMAP and 0.43g of succinic anhydride was added to the solution. After 24 hr, the cPVA was precipitated by adding solution dropwise to 800mL isopropyl alcohol. The solid cPVA was collected by vacuum filtration. This precipitate was redissolved in 60mL methanol, reprecipitated, and vacuum filtered again. Finally, the cPVA was dried under vacuum at room temperature

SWNT/Sodium cholate: A 2wt% sodium cholate aqueous solution was prepared. Nanotubes were added to achieve a final concentration of 0.5 mg/mL. The mixture was sonicated for 2h at 40% amplitude (~10watts) in an ice bath. The resulting suspension was centrifuged for 4 hr at 30,000 RPM and the supernatant was stored for later use.

SWNT/cPVA: Sodium cholate/SWNT solution was added dropwise to a stirred 10wt% cPVA aqueous solution. 10 min after addition, the mixture was put into a dialysis tube (MWCO 10,000) and a 24hr dialysis was performed in distilled water.

Synthesis of SWNT/cPVA -Protein A: 0.5mL of cPVA solution was mixed with 125μl 33.4 mg/mL EDC and 175μl 24.2 mg/mL of NHS for 2h. Residual EDC and NHS was removed using spin dialysis tubes with settings of 50 min and 250 rcf. Protein A was added to achieve a final

concentration of 500μg/mL and stirred for 2 hrs. Free protein A was removed using a spin dialysis tube with an appropriate molecular weight cutoff.

Synthesis of carboxymethylated phenoxy dextran (CMPD): 8g of Carboxymethylated dextran was dissolved in 60 mL of 1N-NaOH solution. 6.65g of 1,2-Epoxy-3-phenoxypropane was added to the dextran solution at 25°C. The resulting mixture was stirred for 10 h at 40°C. CMPD was precipitated with an excess of methanol and then filtered. In order to completely remove other reagents, CMPD was dissolved in 20 mL water, and then precipitated again with an excess of methanol. This purification was carried out three times.

Synthesis of Dialyzed SWNT/CMPD: 2.9mL of 2wt% Sodium Cholate/SWNT was mixed with a weight of CMPD 250 times the weight of SWNT. SWNT weight was determined by UV absorption at 632 nm. The solution was added to a Pierce dialysis unit with molecular cutoff of 3500. The dialysis was carried out in 2L of stirred water for 24hr with the buffer changed at least once. The sample was then removed and centrifuged for 90 minutes at 16000g. The supernatant was stored at 4°C until further use.

Synthesis of Sonicated SWNT/CMPD: 20mg of CMPD, 10mL water, and 10mg of SWNT were mixed. This solution was sonicated for 10 minutes at 10W while keeping the sample on ice. The resulting solution was then centrifuged for 90 minutes at 16000g. The supernatant (approximately 90% of solution) was kept. The centrifugation was then repeated, keeping only about ~70% of solution. The supernatant was stored at 4°C until further use.

Synthesis of SWNT/CMPD-Protein A: Protein A was attached to the CMPD through EDC/NHS chemistry. Briefly, 40μl of EDC (0.176M) and 40μl of NHS (0.263M) was added to 1mL CMPD/SWNT. The solution was stirred for 30 minutes at room temperature. Spin dialysis was then performed for 10 min at 13,000 RPM. Next, Protein A dissolved in 1mL PBS (pH 8) was added for a final Protein A concentration of 400μg/mL. This solution was gently stirred at room temperature for 2 hours. The free protein and polymer was filtered out using a dialysis membrane of with a cutoff of 100kDA. The final SWNT concentration was measured and samples were stored at 4°C until further use.

Synthesis of SWNT/PLPEG-COOH: 10g of PLPEG-COOH was added to 10 mL of water, and then 5 mg of SWNT was added. The mixture was sonicated for 20 min at a power of 10W in an ice bath. The resulting solution was centrifuged for 3 h at 16,000g and the supernatant was stored.

Synthesis of SWNT/PLPEG-COOH -Protein A Complex: The carboxylic acid of PLPEG-COOH was coupled to amino groups on Protein A. 1mL of SWNT/PLPEG-COOH at a concentration of 25μg/mL was prepared. This was stirred with EDC-HCl (3.5 μM) and NHS(4,914 μM) for 1.5 h at 25C. Excess EDC and NHS was removed using a centrifugal filter device (Amicon Ultra-4, MWCO 10 kDa). The SWNT/PLPEG-COOH-Protein A was resuspended in PBS and recentrifuged twice. Protein A was then added for a final concentration of 300μg/mL. The solution was gently stirred for 2 h at 25°C and 10 h at 4°C.

Synthesis of DNA/SWNT-Protein A Complex: DNA SWNT were synthesized following Zhang et al. $d(AT)_{15}$ and $d(GT)_{15}NH_2$ oligonucleotides were obtained from (Integrated DNA Technologies). Briefly, 2mg/mL Nano-C SWNT with 1mg/mL DNA was mixed in a 0.1 M NaCl solution. The mixtures were sonicated with a 3 mm probe tip (Cole-parmer) for 10 min at a power of 10 W. Samples were then centrifuged for 3 hours at 16,000g. Finally, the supernatant was collected.

Suspension of Nanotube with Chitosan: Chitosan (0.25 wt% to water) was dissolved in water containing 1 vol% acetic acid. 20 mg of nanotube was mixed with 10 mL of the chitosan solution. The resulting mixture was sonicated for 45 min at 40% amplitude (10 watts) in the ice bath using a probe-tip sonicator. The SWNT/chitosan solution was centrifuged for 3 h at 16,000 g using a tabletop centrifuge. Only ~70% of the supernatant was removed. The new liquid was centrifuged for 3 h at 16,000 g and the supernatant was removed in the same manner.

Preparation & Modification of SWNT-Chitosan Array: 375 μl of SWNT/chitosan suspension was well mixed with 125 μl of 2wt% chitosan in a 1 vol% acetic acid solution. SWNT/chitosan solutions containing 10-100μg/mL SWNT were used. This solution was cross-linked using 2.8 μl of 50 vol% glutaraldehyde. 3μl of this solution was spotted on a patterned glass slide (4x6 spots). The cross-linking reaction proceeded in a humidified chamber for 15 h at 25°C. The chip was washed with H_2O for 15min, with 0.01 M solution of NaOH for 15min, and again with H_2O for 15min. The last water wash was done twice, for a total washing time of one hour. To

introduce carboxylic acid to chitosan, 450 mg of succinic anhydride was dissolved in 45mL of water and the resulting solution was added to the chip. After the reaction proceeded for 5 h at 25°C, the array was washed 4 times with water for one hour. To activate the carboxylic acid on the array, 863 mg of EDC and 575 mg of NHS were dissolved in 45 mL of water, and then the resulting solution was added to the array for 2 h at 25°C. The array was then washed with water four times in one hour. Then the chips were left in humidified chambers overnight with a 33 mM solution of NTA in PBS at pH 8.0 spotted on top of each hydrogel. After washing the chip 4 times with water in one hour, 45 mL solution 100mM $NiSO_4$ was added to the array for 1 h at 25°C. The array was then stored in the nickel solution or in water for later analysis.

Spectroscopy and Microscopy: Near-infrared photoluminescence spectra were acquired on a custom inverted microscope, the Zeiss D.1 Observer. The SWNT are excited by a 785nm laser, from B&W Tek, and the emission is sent to the Princeton Instruments Acton SpectraPro 2500i Spectrograph spectrometer and the Intervac MOSIR Camera 350 near infrared camera. Absorption measurements were taken with a Shimadzu UV-3101 PC UV-VIS-NIR scanning spectrophotometer.

Spectral Deconvolution: A custom Matlab script was used to deconvolute raw spectra by minimizing the difference between the raw spectrum and a linear combination of spectra from nanotube species.

Solution phase nanotube response assay: 200µl aliquots of SWNT/polymer-Protein A complex were put into a 96-well plate at an approximate concentration of 1mg/L. Antibody solution, typically 60µl, was then added to each well. Spectra were taken before and 24 hours after addition of antibody solution in order to quantify quenching. The change in signal due to dilution of the SWNT complex was subtracted out from the final data. Calculated standard deviations took into account the variation in the measured control experiments that only looked at the effect of dilution.

Hydrogel nanotube response assay: A 50x/0.7 Zeiss objective was used to image hydrogels on a glass slide. A typical experiment was run for approximately 30 minutes with a data point collected as the integrated emission spectra for every 10 seconds. 20µl of PBS was added to

each spot on the hydrogel after it was removed from a storage container. After turning on the laser and allowing signal stabilization 100mM $NiSO_4$ was added for a final concentration of 50mM. This served as a control to verify that the known potent SWNT quenching of Ni^{2+} could be observed. The Nickel was then washed away with PBS, leaving 20µl of PBS on the gel. 20µl of 0.5mg/ml His-tag protein A was then added to the gel. After 5 minutes of equilibration the spot was washed. 20µl of analyte antibody or control protein was then added. These analytes included human IgG, mouse IgG, rabbit IgG, guinea pig IgG, anti-histag antibody, YPD, and BSA. Data was collected for at least 5 minutes after analyte addition. Washing steps consisted of aspiration of liquid from the hydrogel spot, addition of 20µl of PBS, aspiration, and addition of 20µl of fresh PBS. Care was taken to minimize contact with the stage during addition and washing steps.

Because the gel was found to be sensitive to ions in the buffer, PBS exactly matching Invitrogen's PBS formulation for antibodies was used. It was composed of 3g of NaCl, 111mg of KH_2PO_4, and 582mg of Na_2HPO_4 dissolved in 500mL of water.

Histagged EGFP Fluorescence Assay: A white light source was used with a Zeiss AxioCam MRm imaging camera and a 633nm high-pass filter to illuminate a SWNT/chitosan hydrogel synthesized on a glass slide. A 50X Objective was used and images were collected using Zeiss Imaging Solutions AxioVision software with an exposure time of 150ms.

Materials: Two types of SWNT were purchased: CoMoCat 'SWeNT SG 65' from SouthWest Technologies and Nano-C from the company Nano-C. Protein A, Human IgG, Goat IgG, Rabbit anti-Mouse IgG, Mouse IgG were purchased from Invitrogen.

Guinea Pig IgG was purchased from Santa Cruz Biotechnology.

Distearoyl-*sn*-glycero-3-phosphoethanolamine-N-[carboxy(polyethylene glycol)-2000] (ammonium salt) (PLPEG-COOH) was purchased from Avanti Polar Lipids Inc.

NMP, PVA (Mw 13,000-23,000), DMAP, Succinic anhydride, Sodium cholate, Chitosan (low molecular weight 448869), $NiSO_4$ hexahydrate, Acetic acid, Nα,Nα-bis(carboxymethyl)-L-lysine, Phosphate Buffered Saline, glutaraldehyde, *N*-(3-dimethylaminopropyl)-*N'*-ethylcarbo diimide hydrochloride (EDC·HCl), *N*-hydroxysuccinimide (NHS), Sodium hydroxide, Hydrochloric acid,

BSA, anti-histag antibody (H1209), 1,2-Epoxy-3-phenoxypropane, methanol, and isopropyl alcohol were purchased from Aldrich.

$(AT)_{15}NH_2$ and $(GT)_{15}$ oligonucleotides were purchased from Integrated DNA Technologies.

6X4 spot glass slides were purchased from Tekdon.

5. Experimental Results

5.1 Native Gel

Native gels were used to confirm that Protein A binds to the IgG used in experiments. Both mouse and human IgG showed binding to protein A, as shown in Figure 5. Figure 6 shows that Guinea pig and rabbit IgG also show binding.

Figure 5: Native Gel showing that Human IgG and Mouse IgG bind Protein A. Lane 1 is a standard. Lane 3 is Protein A alone. Lane 4 is Mouse IgG alone. Lane 6 is Protein A and Mouse IgG. Lane 7 is Human IgG alone. Lane 9 is Human IgG and Protein A. Lanes 5 and 8 were an attempt to check for binding of SWNT/polymer-protein A to the IgG, but are not readily distinguishable from lanes 4 and 7, respectively, where only IgG was run. Lane 2 has just the SWNT/polymer-protein A.

Figure 6: Native Gel showing that Guinea Pig IgG and Rabbit IgG bind Protein A. Lane 1 is a standard. Lane 3 is Protein A alone. Lane 4 is Guinea Pig IgG alone. Lane 6 is Protein A and Guinea Pig IgG. Lane 7 is Rabbit IgG alone. Lane 9 is Rabbit IgG and Protein A. Lanes 5 and 8 were an attempt to check for binding of SWNT/polymer-protein A to the IgG, but are not readily distinguishable from lanes 4 and 7, respectively, where only IgG was run. Lane 2 has just the SWNT/polymer-protein A.

5.2 Direct Suspension by Dialysis

Protein A suspension was improved at higher pH, as seen in Figure 7. There was highly visible aggregation for pH 3 and pH 5. Recovery of suspended SWNT after centrifugation was low for all the samples except for pH 9.5, which shows SWNT concentration close to that of the initial SC/SWNT suspension used, as seen in Figure 8. Unfortunately, even the SWNT suspensions prepared at pH 7 or 9.5 were only metastable. The solutions flocculated when they were put into chitosan for hydrogel preparation, as shown in Figure 9 and aggregated by themselves over a period of days.

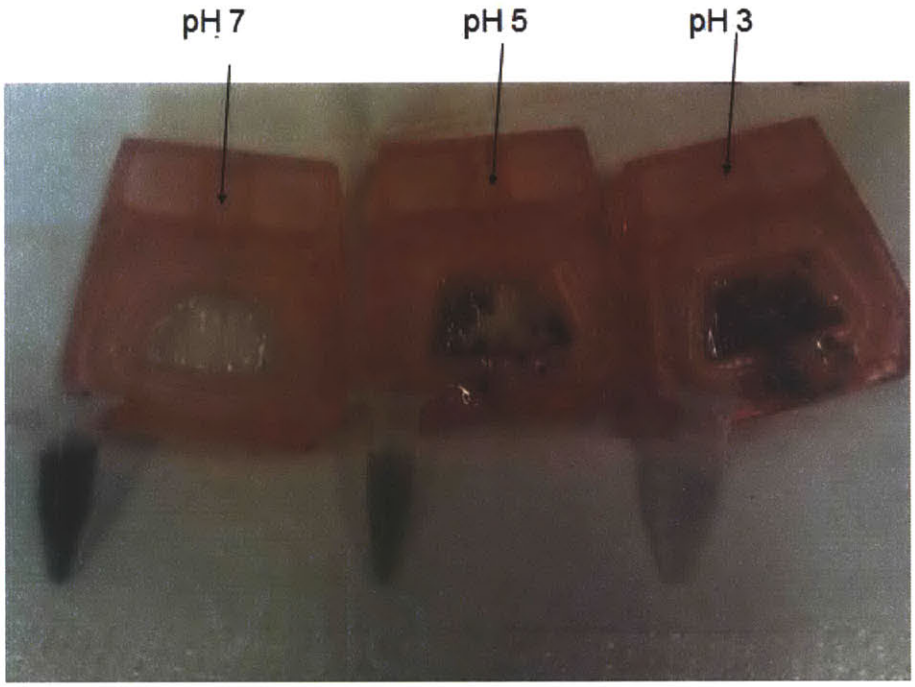

Figure 7: Nanotube solutions and dialysis cartridges without aggregated nanotubes after dialysis with varying pH.

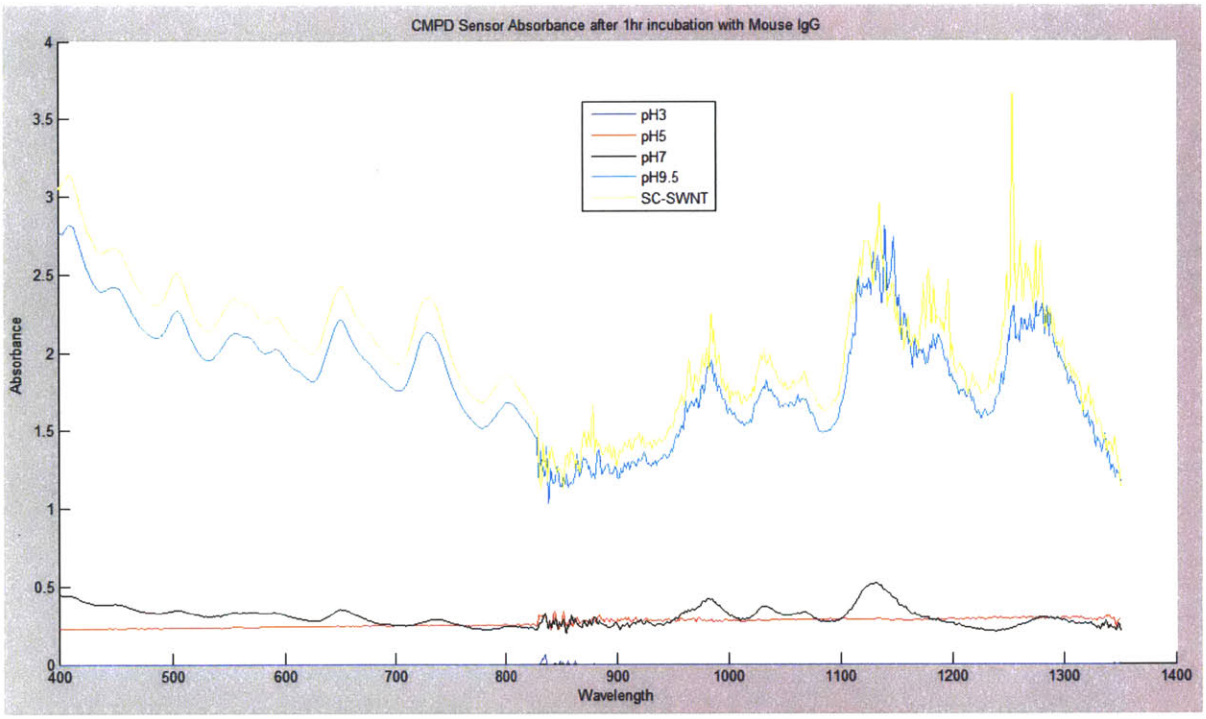

Figure 8: Absorption spectrum of SWNT/Protein A samples recovered after dialysis at various pH conditions.

Figure 9: Aggregated nanotubes in chitosan gel after suspension directly with protein A at a high pH.

5.3 Carboxy methyl phenoxy dextran

Evidence that SWNT was successfully functionalized with protein A is shown in Figure 10, which shows the photoluminescence spectrum before and after protein A functionalization.

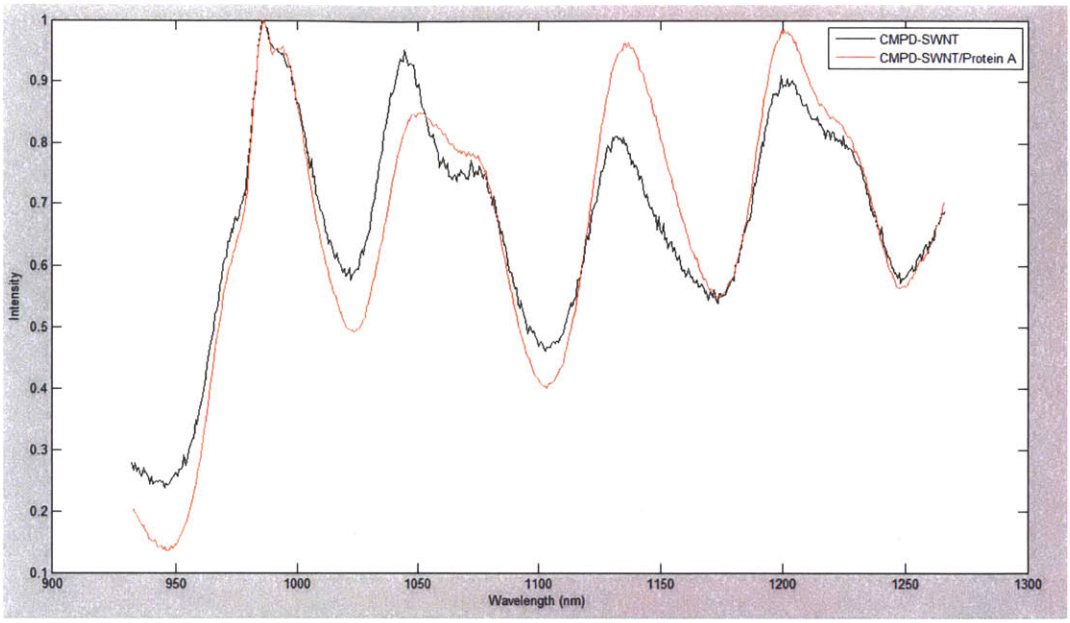

Figure 10: Excitation-emission spectrum with normalized intensity versus wavelength for SWNT/CMPD (black) and SWNT/CMPD-Protein A (red). The spectral shift and relative intensity shift of some peaks is evidence of functionalization.

A series of sample spectra are shown in Figure 11. In each of the 36 panels the upper blue curve is an excitation-emission spectrum taken before addition of antibody. Each of the lower red curves is an excitation-emission spectrum taken after addition of antibody, and the sensor shows clear quenching in this case.

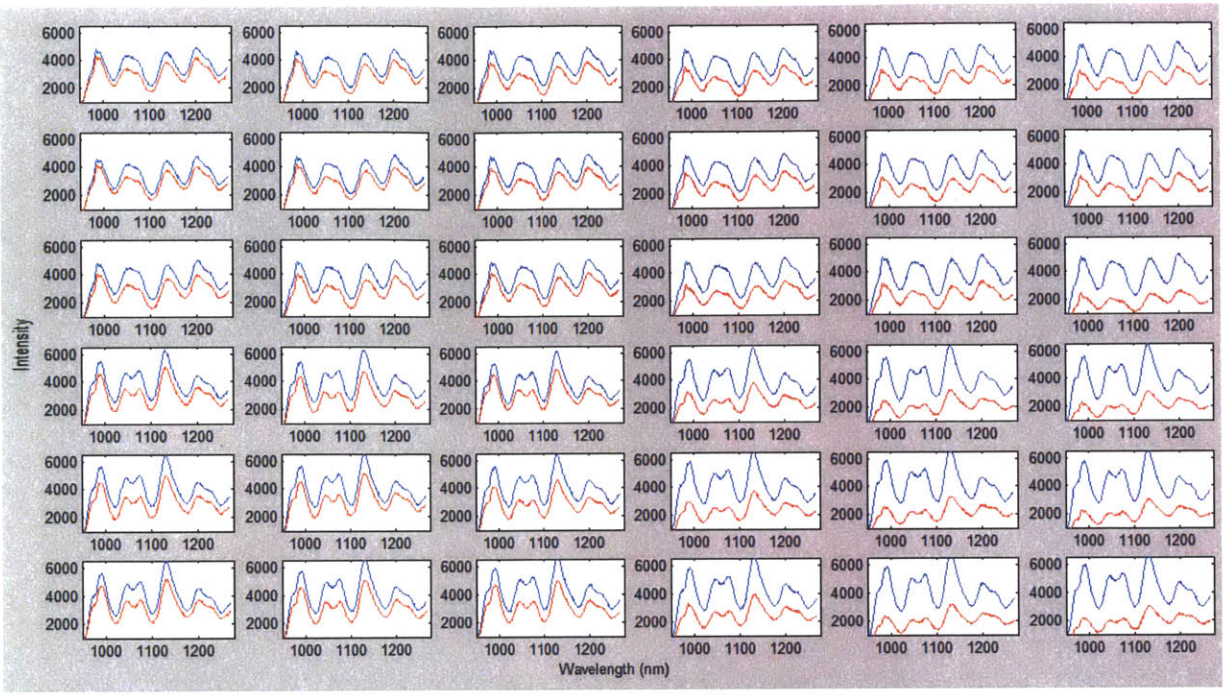

Figure 11: 36 graphs of near-infrared photoluminescence spectra. All graphs are intensity (a.u.) versus emission wavelength (nm) with blue curves corresponding to control measurements and red curves corresponding to measurements 24 hours after Rabbit IgG addition. Antibody concentration increases left to right, and it can be seen that the red spectra have considerably lower intensity to the right. There is no relation between the rows.

The concentration dependent response of photoluminescence to IgG was probed using mouse IgG, human IgG, guinea pig IgG, and rabbit IgG. Results for rabbit IgG and human IgG are shown in Figure 12 and Figure 13 respectively. Note that the error bars are approximately the same size in both graphs, but the averaged response for Human IgG is close to zero for all tested concentrations.

The fitted curves for each nanotube in Figure 12 are derived from considering the reaction Ab+SWNT ⇔ SWNTAb. Even at concentrations as low as 1nM of Ab, [Ab]>>[SWNT], because [SWNT] was around 100fM.

$$\frac{d[SWNTAb]}{dt} = k_{on}[\mathrm{Ab}][\mathrm{SWNT}] - k_{off}[\mathrm{SWNTAb}]$$

Given that Ab~Ab_0, an expression for the fractional quenching, y, in the system at equilibrium as a function of the initial antibody concentration and the apparent sensor K_d is

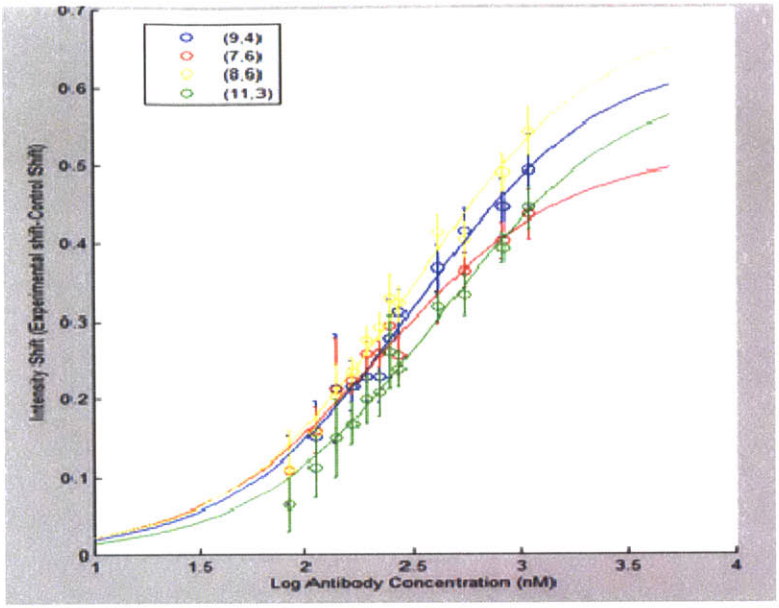

Figure 12: The protein A-dextran/SWNT quenching response for polyclonal rabbit IgG is graphed for 4 different SWNT species. The solid line fits the data based on the reaction IgG+SWNT ←→ SWNTIgG. The fitted K_d values are in the range 230-430nM.

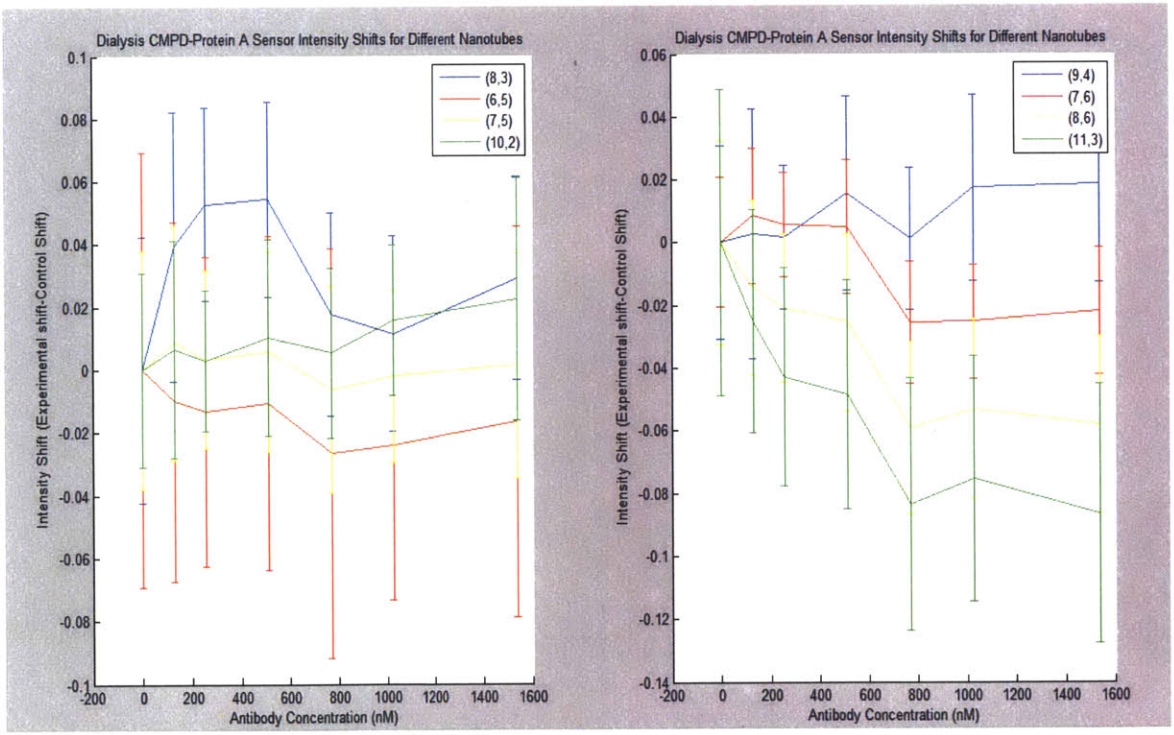

Figure 13: The protein A-dextran/SWNT quenching response for polyclonal human IgG is graphed for 8 different SWNT species. The lines connect consecutive points and are meant to aid the reader in looking for a concentration dependent trend.

Quenching responses for the SWNT/CMPD construct with and without Protein A are shown in Figure 14 for IgG from three different species. There is a significantly larger response to Mouse IgG for the protein A sensor, but the nonspecific interaction of the antibody with the SWNT/CMPD caused the abandonment of further work with this polymer system.

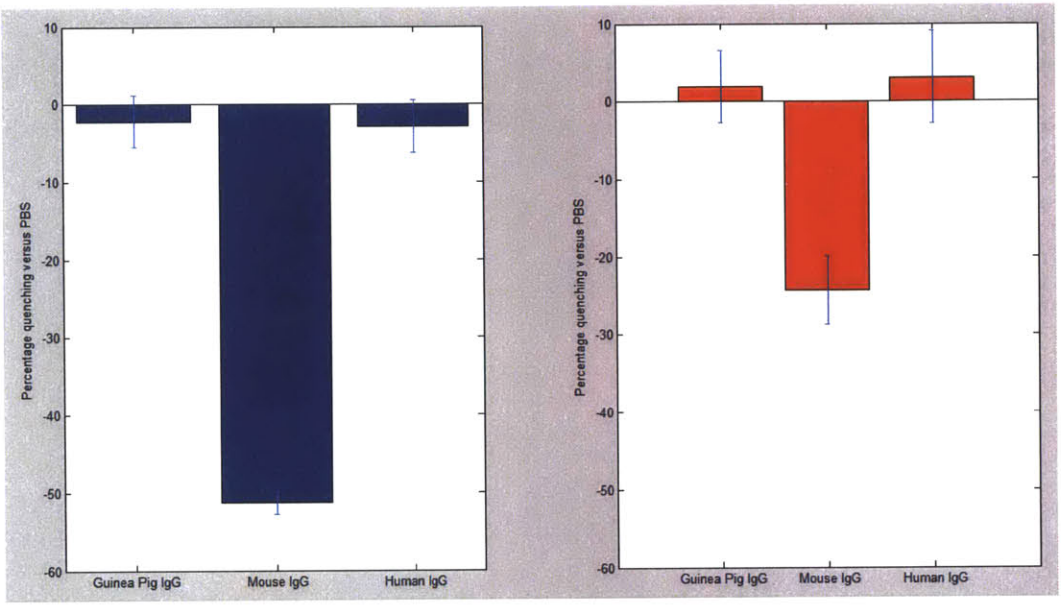

Figure 14: Percentage quenching versus PBS after addition of Guinea Pig IgG, Mouse IgG, or Human IgG to SWNT/CMPD-Protein A(left) or SWNT/CMPD (right).

5.5 cPVA

The cPVA sensor, before and after functionalization with protein A, was tested for a response to guinea pig IgG, mouse IgG, and Human IgG. The results are shown in Figure 15. There is similar quenching for guinea pig and human IgG, whereas the quenching for mouse IgG is about double for the protein A version.

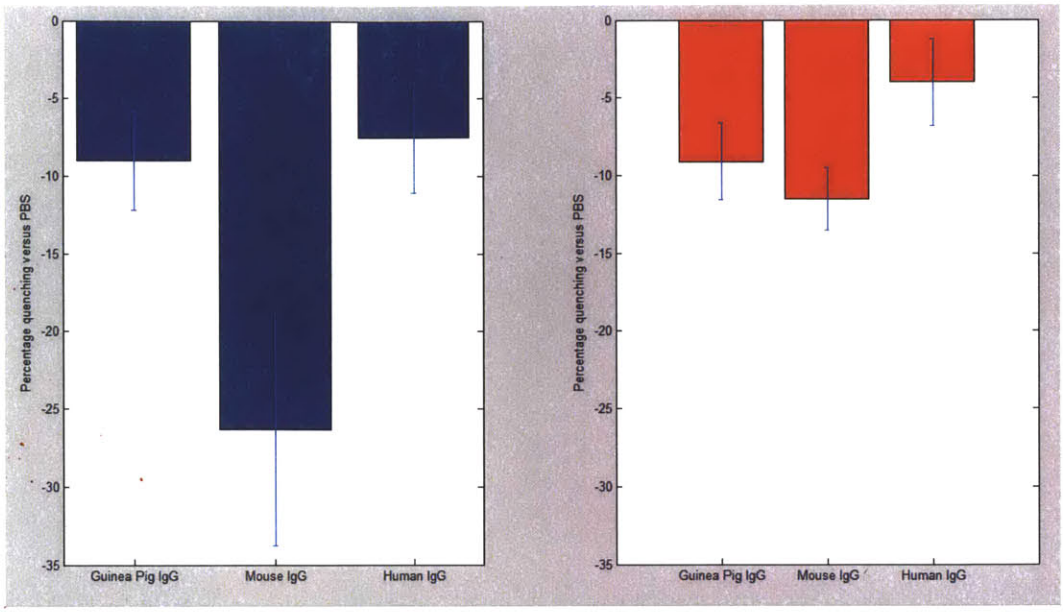

Figure 15: Percentage of signal quenched by addition of Guinea Pig IgG, Mouse IgG, and Human IgG to SWNT/cPVA-Protein A (left) and SWNT/cPVA (right). The sensor was made starting with purified (6,5) nanotube.

5.6 DNA

DNA polymers for suspending SWNT were explored first without conjugation of Protein A. Figure 16 shows the responses of $(AT)_{15}NH_2$ and $(GT)_{15}$ oligonucleotide suspended SWNT to multiple IgG. There are significant responses for most of the tested IgG. Interestingly, the response to Human IgG is qualitatively different: there is a decrease in intensity after addition for the oligonucleotide with adenine but an increase in intensity after addition for the oligonucleotide with guanine.

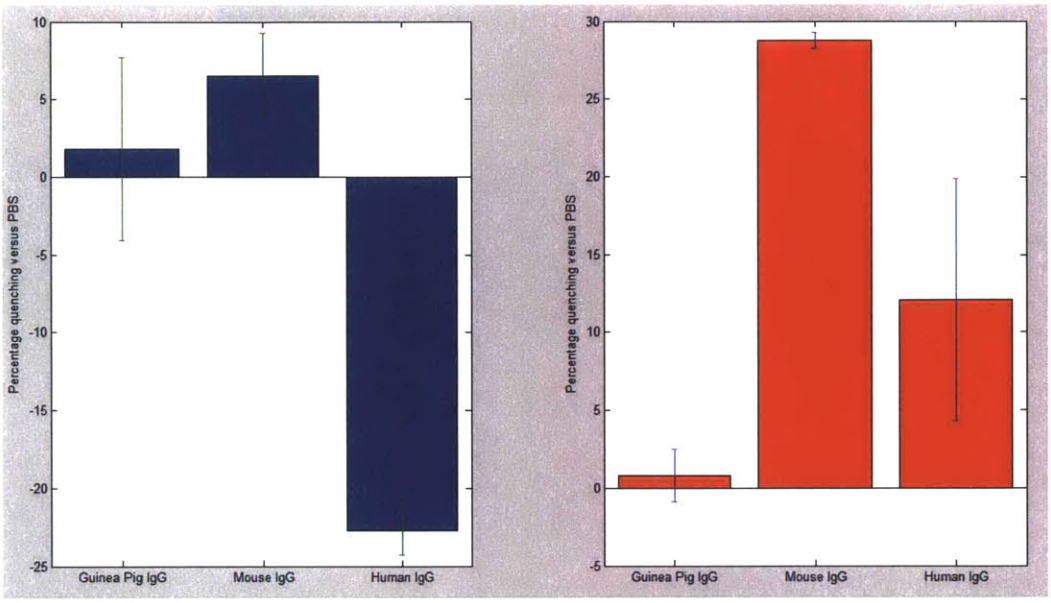

Figure 16: Percentage of signal quenched by addition of Guinea Pig IgG, Mouse IgG, and Human IgG to $(AT)_{15}$/SWNT (left) and $(GT)_{15}$NH2/SWNT (right). This graph is for the deconvoluted (6,5) nanotube. Other nanotubes show similar quenching.

5.7 PLPEG-COOH

PLPEG-COOH is a carboxylated lipid which was previously shown to suspend nanotubes and allow for conjugation of functional proteins via NHS/EDC chemistry (Jong-Ho Kim 2010). Figure 17 shows the results of screening the PLPEG-COOH construct with four different antibodies. Work on this sensor was not continued because of issues with nonspecific interaction which are not shown here.

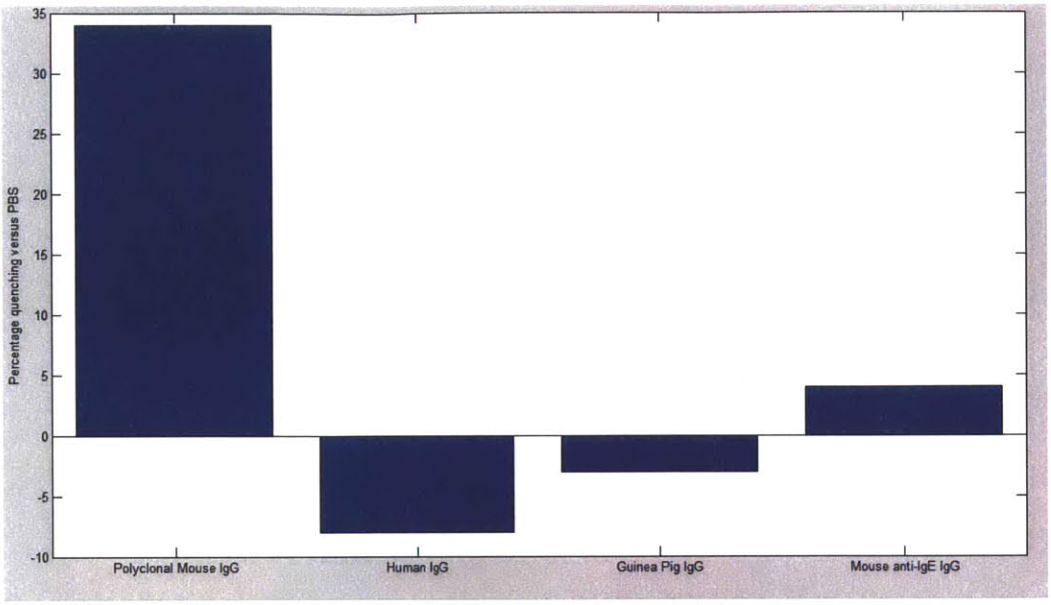

Figure 17: Percentage of signal quenched by addition of Guinea Pig IgG, Mouse IgG, Human IgG, and Mouse anti-IgE IgG to SWNT/PLPEG-COOH-Protein A. This graph is for the deconvoluted (6,5) nanotube. Other nanotubes show similar quenching. Data is from a single run.

5.8 Chitosan Nickel Hydrogel

Chitosan is a copolymer of β-(1→4)-linked 2-acetamido-2-deoxy-D-glucopyranose and 2-amino-2-deoxy-D-glucopyranose, and it is generally obtained from deacetylating crustacean exoskeleton. A common definition of a hydrogel is a 'macromolecular network swollen in water or biological fluids' (J. Berger 2004).

Chitosan nickel chips were synthesized according to a modified procedure of that previously published by Jin-Ho et al. (Jin-Ho Ahn 2011). The steps are outlined in Figure 18. The final product is an array of gels, as seen in Figure 19, which can be assayed for response to IgG and other proteins.

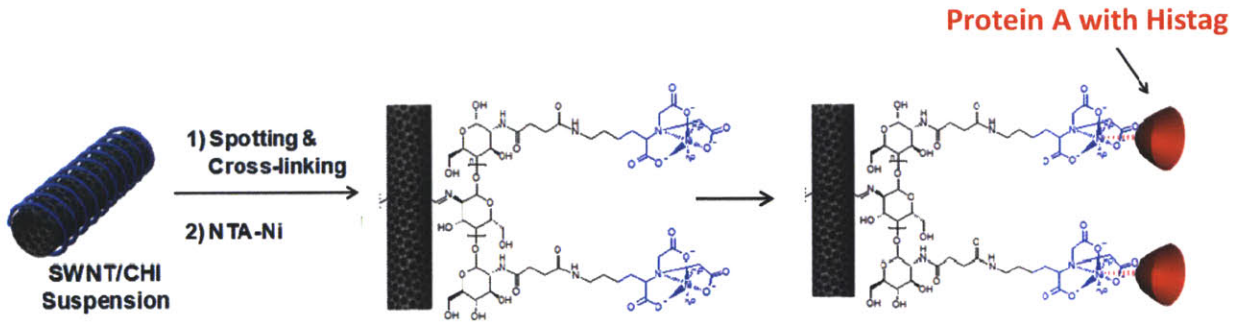

Figure 18: Synthesis scheme for making the chitosan nickel hydrogel. SWNT/CHI are first spotted on a chip and crosslinked. After carboxylation, NTA is attached to the chitosan via EDC/NHS chemistry. Nickel is then added. Finally, the histagged Protein A, shown here in red, is added to the complex. Figure is modified from (Jin-Ho Ahn 2011)

Figure 19: 50X objective imaging a SWNT/Chitosan-NTA/Ni-Protein A hydrogel. There are 16 separate hydrogels on this chip. A faint red color from the 785nm laser is visible from the objective.

Significant difficulties were encountered in obtaining an excitation-emission spectrum which showed the well established quenching behavior caused by Ni^{2+} ions (Jonathan Brege 2009). It was found that great care was necessary in order to eliminate glutaraldehyde and succinic anhydride present after cross-linking and succinylation steps respectively, in order to restore the Ni^{2+} quenching observed in the original chitosan suspended SWNT. Another significant experimental change was the use of SWNT in higher proportion relative to chitosan in the gel. This increased the starting intensity count and minimized the effect of noise.

A sample real-time data run, where signal from the chitosan hydrogel is collected every 10s, is shown in Figure 20. This procedure follows that of Reuel et al (a paper from the Strano lab currently under review). After Ni^{2+} quenching of the gel is shown, histagged Protein A is added, causing a dramatic increase which is sustained after washing. There is a similar increase after addition of human IgG. Simple addition does not cause any response. The final addition is anti-histag antibody, which consistently shows a response.

Figure 21 shows a calibration curve for SWNT/Chitosan-NTA/Ni-Protein A complex with human IgG. Each point represents an average of multiple runs like the one in Figure 20. There is a roughly sigmoidal response with a K_d that appears to be on the order of 100nM.

Figure 22 shows a control where histagged EGFP is added instead of histagged Protein A. If the quenching is due to binding of IgG with protein A, no response, or at least no response with a K_d similar to that of the for SWNT/Chitosan-NTA/Ni-Protein A complex is expected. However, there is a clear response of the gel with the hisEGFP to the addition of IgG which is on the same order of magnitude (10%) as the response of the gel with the hisProtein A.

Figure 23 shows a control where BSA is added to a chitosan hydrogel prepared with the histagged Protein A. For comparison, at this concentration of BSA, the human IgG calibration curve shows that human IgG would cause about a 15% response. The BSA response at this concentration was 7%±3%.

The hydrogel construct was also shown to give a large response upon addition of the yeast culture media YPD, which contains a diverse set of ions, lipids, carbohydrates and peptides from yeast extract.

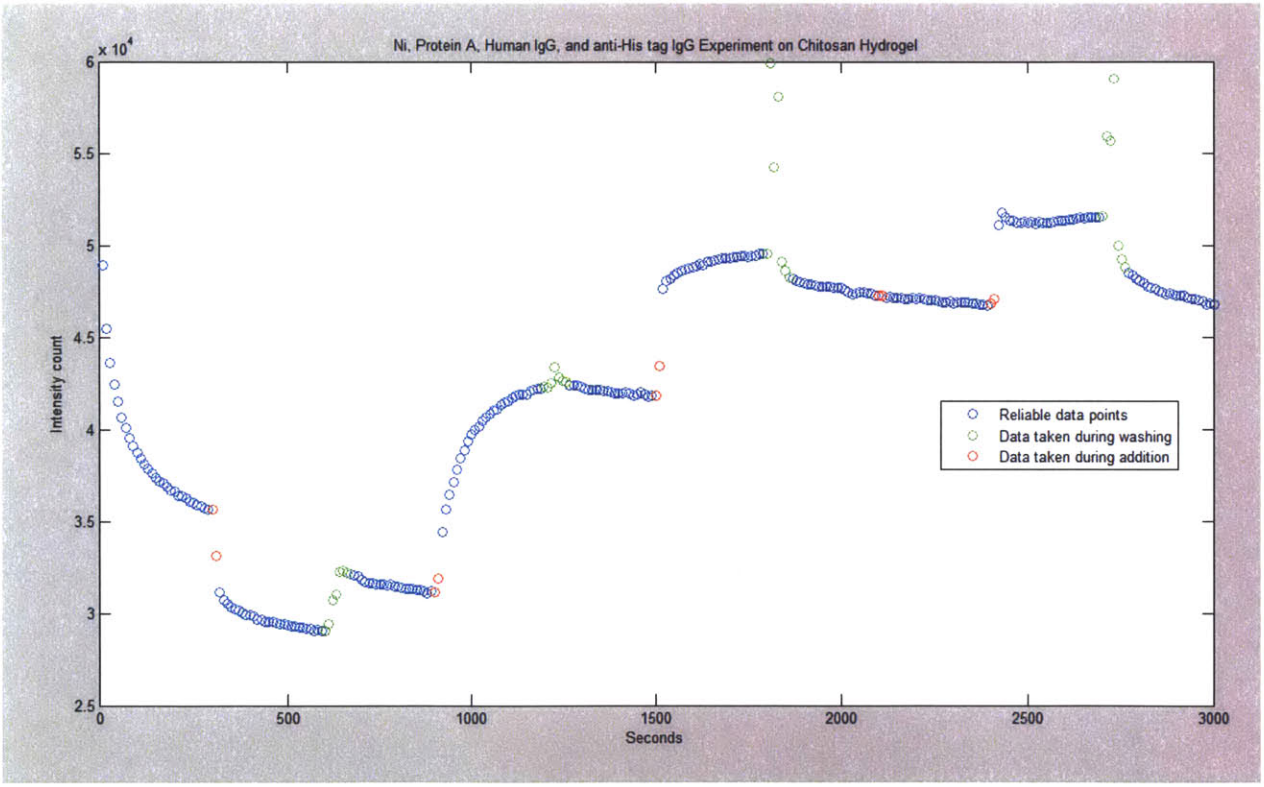

Figure 20: Sample data run showing emission intensity at 996nm over time with addition of human IgG to the chitosan array with histagged Protein A. Red points represent addition of Ni, Protein A, 1g/L (6μM) Human IgG, PBS, and anti-histag Antibody. Green points represent washing steps. Blue points are all other data points. Exposure time is 10s.

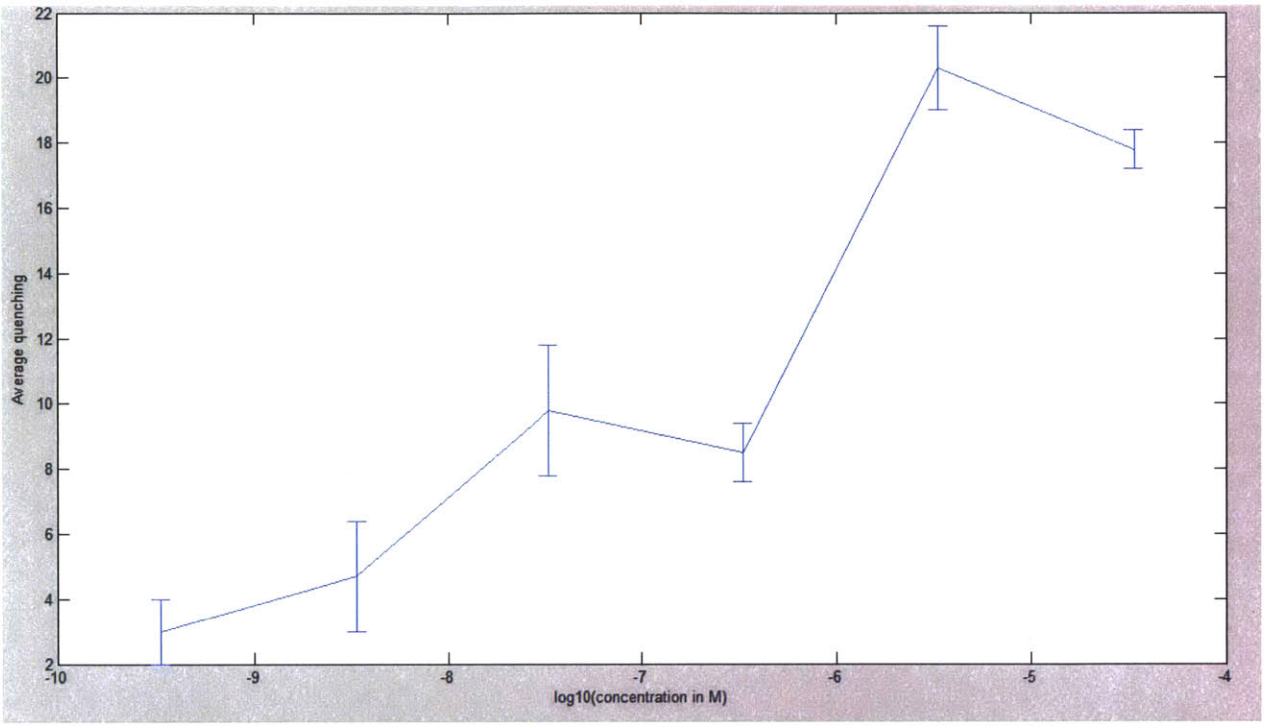

Figure 21: SWNT/Chitosan-NTA/Ni Protein A calibration curve for Human IgG. Quenching is graphed versus the $\log_{10}$ of the molar concentration

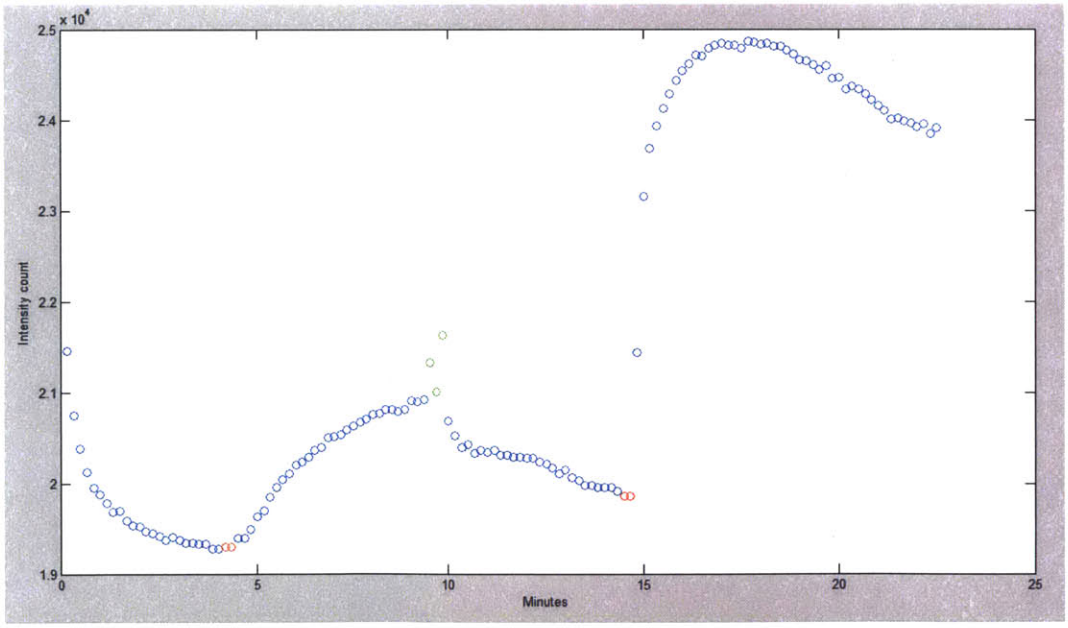

Figure 22: Sample control run showing emission intensity at 996nm over time with addition of human IgG to the chitosan array with histagged EGFP. Red points represent addition of Protein A, and Human IgG. Green points represent washing steps. Blue points are all other data points. Exposure time is 10s. The nickel addition and washing step is not shown.

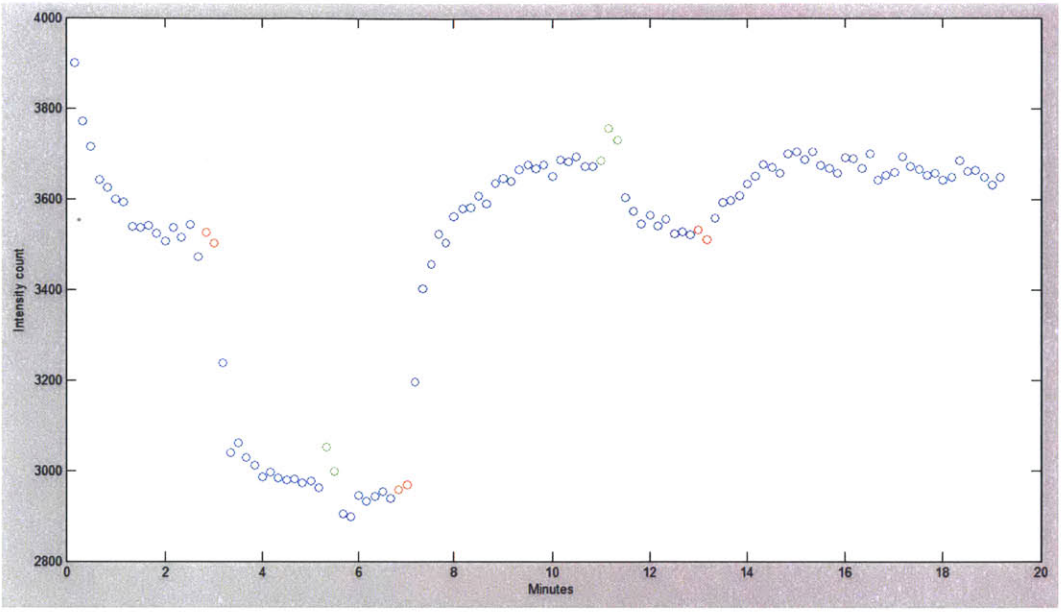

Figure 23: Sample data run showing emission intensity at 996nm over time with addition of human IgG to the chitosan array with histagged Protein A. Red points represent addition of Ni, Protein A, and .001g/L (6nM) Human IgG. Green points represent washing steps. Blue points are all other data points. Exposure time is 10s.

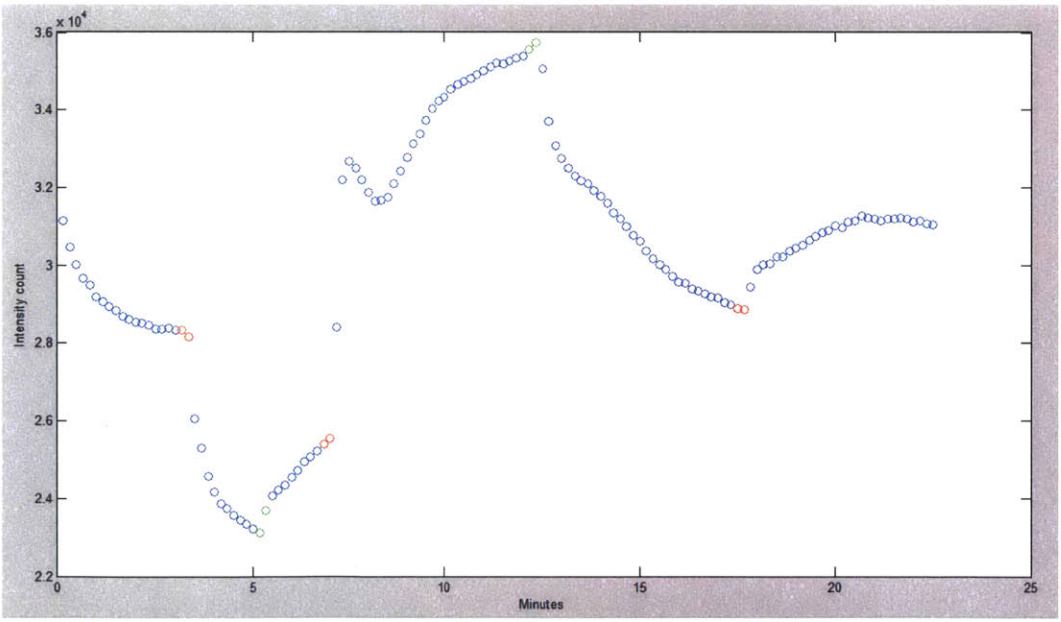

Figure 24: Sample data run showing emission intensity at 996nm over time with addition of BSA to the chitosan array with histagged Protein A. Red points represent addition of Ni, Protein A, and .5g/L (6μM) BSA. Green points represent washing steps. Blue points are all other data points. Exposure time is 10s.

Figure 25 shows histagged EGFP fluorescence after a series of washing steps. It appears that no additional fluorescence is retained on the gel with the NTA/Ni compared to the gel with only NTA. This was an unexpected result, and indicates that either the NTA group is not being

attached to the chitosan during the synthesis or there is so little of it that the EGFP retained by binding to NTA/Ni cannot be resolved over the fluorescence attributable to nonspecific binding.

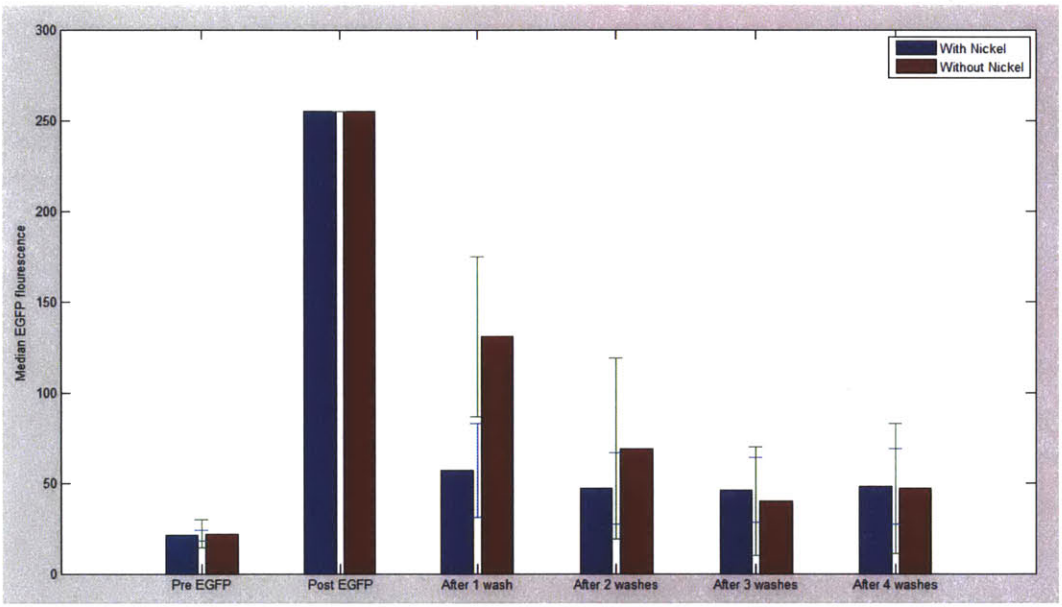

Figure 25: Histagged EGFP fluorescence from chitosan hydrogels before addition of EGFP, after addition, and after 1,2,3,or 4 washing steps with PBS. Washing steps are identical to those used in the real time traces.

Washing steps, where liquid on the chitosan gel was aspirated, replaced with 20µl PBS, aspirated, and replaced with 20µl PBS, reduced the signal from either histagged proteins or IgG after 2 minutes as shown in Figure 26. Each washing step was presumed to eliminate nonspecific binding of proteins.

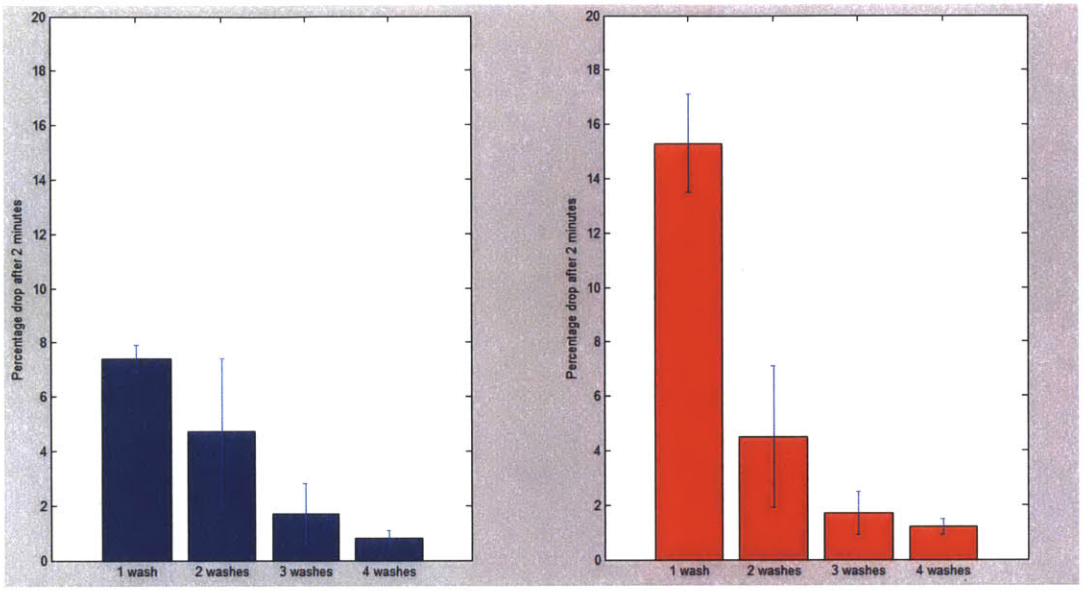

Figure 26: Percentage drops in near-IR signal 2 minutes after washing hydrogels 1,2,3, or 4 times after addition and 10 minute incubation with histagged proteins (left) or IgG(right).

6. Discussion

A substantial amount of the quenching observed for the SWNT/cPVA and SWNT/CMPD constructs does not depend on Protein A. One possible source of nonspecific interaction between the antibody and the SWNT/polymer construct could be electrostatic forces. The dominant subcomponents of the pooled human IgG are IgG1 and IgG2, which have isoelectric point (pI) values of 8.6$\pm$.4 and 7.4$\pm$.6 respectively (Hamilton 2001). Therefore, we expect the human IgG to be positively charged at the neutral pH of experimental conditions. Polyclonal mouse IgG has been reported to possess a pI of 5.5-8 (Hamilton RG 1987). The Mouse IgG would therefore be more of a mix of positive and negatively charged antibodies. At a neutral pH all the polymers are expected to be negatively charged before attachment of protein A, and even more negatively charged after that, because the recombinant Invitrogen protein A has a pI value of 5.2. Based on this reasoning, it seems unlikely that the driving interaction is electrostatic, since the mouse IgG should have less affinity for the more negative surface than the human IgG, but it has more for both the SWNT/cPVA and SWNT/CMPD.

In the case of human IgG the addition of protein A to SWNT/cPVA or SWNT/CMPD does not significantly alter the response. However, for the mouse IgG there is significantly more quenching in both cases. There is evidence from the native gel that the tested proteins do bind to protein A, so it is not likely that most of the protein A is conjugated to the polymer and not interacting with IgG, even if the EDC/NHS chemistry has oriented some of the protein A so that they are sterically inhibited. The photoluminescence spectra offer evidence that the attachment of protein A did take place. There could be something special about the mouse IgG that allows signal transduction to happen after binding. One possible difference between the antibodies is hinge length, since a longer hinge could allow the antigen binding regions of the antibody to wobble around more and interact more frequently with the nanotube. However, the literature shows that human IgG1 and mouse IgG have very similar hinge lengths, so this is an unlikely explanation (Jeffrey L.Dangl 1988).

The SWNT/chitosan hydrogels system currently shows transient signals in control experiments that were not expected based on other work in the Strano lab. Washing appears to return all signals to a baseline level, suggesting that no stable binding to the NTA/Ni is taking place. There may be an unresolved problem with the gel synthesis because there does not appear to be more histagged EGFP retained on hydrogels with NTA/Ni versus just NTA. Transient signal is caused by IgG when added to a hydrogel previously treated with histagged protein A, histagged EGFP, or no other protein. There is also a large response to YPD (about 40%), and a smaller response to BSA (about 7%) from a gel with histagged Protein A. A separate remarkable result is that histagged EGFP was found to cause a large increase fluorescence but is reported to cause a large decrease in fluorescence in Jin-Ho et al.

In order to critically evaluate the transient signals in the real time traces from the chitosan hydrogels, reaction and diffusion time constants can be calculated. The binding interaction of Protein A and IgG has a K_d of about 10nM, with a k_{on} of $2*10^5$ $M^{-1}s^{-1}$ and a k_{off} of .002 s^{-1} (Wells 1996). Assuming no rebinding, this means that the half-life for the complex is about 6 minutes ($t_{1/2}= \ln(2)/k_{off}$) and the reaction takes 25 seconds to reach 99% of equilibrium at typical antibody concentrations ($t=5/(k_{on}*[IgG]+k_{off})$). Therefore, incubation times of 5 minutes are

generally sufficient for specific interaction in an idealized sensor to be observed. Figure 27 shows times till 99% of equilibrium is reached for a range of IgG concentrations, and it can be used to suggest minimum times for experimental runs. It is clear that IgG and protein A reaction is not responsible for observed increases in fluorescence, because even at concentrations of 6nM IgG in Figure 23, where the reaction equilibrium takes >1500s to be established, the response curve levels off in after about 100s.

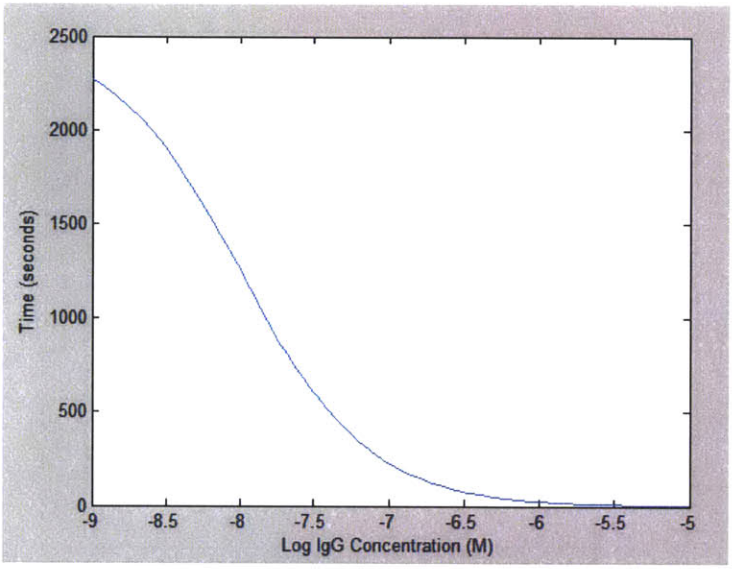

Figure 27: Time to complete 99% of Protein A-IgG formation after additions of various amounts of IgG. Assumes that [IgG]>>[Protein A]

There is relatively little information on the kinetics of hexahistidine-Ni/NTA binding, although the K_d has been estimated as 14nM for a free hexahistdine sequence(Steven Knecht 2008). However, another group reported a hexahistidine tag K_d of 700nM, possibly due to a lowered k_{on} because of steric hindrance(Nieba L 1997). There may be highly significant rebinding in the hydrogel system, given the close proximity of the Ni/NTA groups. With the uncertainty regarding the kinetics of the hexahistidine-Ni/NTA interaction, the probable rebinding, and a K_d~100nM, it seems reasonable to suppose that the kinetics are roughly similar to that of IgG and protein A. Histagged protein was used at a concentration of 500mg/L (11μM), so the reaction is expected to proceed quickly.

The other time constant of interest pertains to diffusion. Diffusivity of Ni in water is $1.2*10^{-5}$ cm^2/s, while it was measured to be between $.03*10^{-5}$ and $.04*10^{-5}$ cm^2/s in 1wt% chitosan

solutions cross-linked with glutaraldehyde weight percentages of 0.1%, 0.5%, or 1% (Krajewska 2001). The diffusivity of the particular proteins used here (EGFP, protein A, IgG) have not been studied in chitosan cross-linked with glutaraldehyde. However, the diffusivities of various small molecules and PEGs are available to suggest values for these proteins, and are presented in Table 1. In the PEG study no diffusion of PEG 4000 through the gel was detected.

Table 1: Diffusivity and sizes of Nickel and PEG. Diffusivity was measured in a 1wt% chitosan gel cross-linked with 0.1% glutaraldehyde. Data from (Olech 1996; Krajewska 2001)

Molecule	Diffusivity (10^{-5} cm^2/s)	Radius (Angstroms)
Ni	0.03	4
PEG 400	0.07	7
PEG 600	0.02	8
PEG 1000	0.009	9
PEG 2000	0.0006	11

The chitosan/SWNT gel was measured to be approximately 0.1mm in thickness, is cross-linked with 0.28% glutaraldehyde and has 0.69wt% chitosan. Using the diffusivity from table 1, an estimated time constant for Nickel diffusion is $t_{0.1mm} \sim L^2/D = (.01cm)^2/(.03*10^{-5}cm^2/s) = 300s$. In experiments, nickel quenching of near infrared fluorescence occurs completely in about 10s.

As can be seen in Table 2, the diffusion coefficients of the proteins of interest in water are approximately the same as the diffusion coefficient of nickel in the hydrogel. In the hydrogel, the diffusion coefficients of the proteins will obviously be significantly smaller. If the diffusivity of PEG 2000 is taken as a generous upper limit on the diffusivity of all the proteins (the molecular weight of all the proteins is an order of magnitude higher than PEG 2000) in the chitosan gel, $t_{0.1mm} = 17{,}000s$. However, there is a near-IR response to these proteins within 10s of addition, which generally increases for approximately ~100s before leveling off. Given that the diffusivity of all of these proteins is probably significantly lower than that of PEG 2000, and that there is some observed response in a time 3 orders of magnitude faster than the calculated $t_{0.1mm}$, it seems unlikely that diffusion is responsible for the observed signals. There may be

large cracks in the gels such that the true pore size is much different than expected with the given chitosan and glutaraldehyde concentrations, or the observed fluorescence changes may be taking place only very close to the interface between the gel and the solution.

Table 2: Diffusivity in water and size of proteins used with the chitosan/SWNT hydrogel.

Sources: a-(Flygare 1971) b-(Ank Valstar 2000) c-(Ingemar Bjork 1972) d-(J.K. Armstrong 2004) e-(Hasemann CA 1989) f-(Gilbert L 2006)

Protein	Diffusivity in water (10^{-5} cm^2/s)	Radius(Angstroms)
BSA	0.06[a]	34[b]
Protein A	0.04[c]	50[c]
IgG	0.04[d]	53[e]
EGFP	0.12[f]	20[f]

There are several studies which have examined diffusion controlled drug release from chitosan scaffolds cross-linked with glutaraldehyde. 5-fluorouracil was encapsulated in 2wt% chitosan fibers through a wet spinning technique where the drug and chitosan solution was extruded into a solution containing 0.25%, 0.5% or 1% glutaraldehyde. Release rates of .01mg 5-fluorouracil /g chitosan/hr were observed for about 4 days after the initial burst release for all glutaraldehyde concentrations. In a separate study, chitosan microspheres containing the small molecule drug theophylline were synthesized by adding glutaraldehyde at a final concentration of 0.3 to 1.6% to an emulsion of 2.7wt% chitosan and theophylline dispersed in a continuous phase of sunflower oil. These microspheres released theophylline at about 5% of encapsulated drug/hr after burst release (Ida Genta 1998). Another study created chitosan sponges 1mm in height with embedded platelet derived growth factor by freeze-drying without any crosslinking, and showed pore sizes of 100μm and protein release over many days (Yoon Jeong Park 2000). Although building a quantitative hypothesis from these studies and other literature as to how quickly nickel and proteins will diffuse through the SWNT/chitosan gel synthesized here is difficult, given the different weights of chitosan and different synthesis procedures, these studies do inform expectations. Specifically, the time scale of hours to days for diffusion of small molecule drugs and a protein out of chitosan constructs suggests that the responses in

the SWNT/chitosan gel from nickel, in about 10s, and proteins, completing in about 100s, may be due to observation of an interface reaction, or to an unexpectedly cracked or porous gel.

Chitosan hydrogels and their applications are reviewed by Berger et al. (J. Berger 2004). The major parameter controlling release of a drug from a hydrogel, and therefore diffusion into the gel as well, is crosslinking density. Logically, the greater the degree of cross-linking the smaller the pore size, due to physical restrictions on previously separate polymer chains. This also means less hydrogel swelling, because amino groups which would otherwise hydrogen bond with water are removed. The pH dependence of swelling seen in some chitosan gels is thought to depend on the protonation of these amino groups, causing chain repulsion. Ionic strength also effects swelling by shielding charges. In a fully cross-linked chitosan gel without amino groups, pH and ionic strength are not major drivers of hydrogel swelling(J. Berger 2004). The chitosan used here was 80% deacetylated, making the molar ratio of amino groups to glutaraldehyde 1:0.93, and since glutaraldehyde reacts with two amino groups almost all of the amino groups will be cross-linked. Partial cross-linking, or electrostatic interactions of the hydroxyl groups present on each chitosan monomer, do leave open the possibility that the proteins are causing a change in hydrogel structure through changing the local pH or ionic strength through diffusion of smaller species, which then alters the quenching of the SWNT. The diffusivity of buffer ions is very close to that of Ni in the chitosan hydrogel (Krajewska 2001), while hydrogen ions may be able to move significantly faster (Sudipto K. De 2002), making diffusion time constants for ionic and pH mediated effects roughly consistent with the time scales of quenching observed in Figure 20-24.

As an alternative to using values of diffusion coefficients found in literature, there are several theoretical frameworks which have been employed to model diffusive transport in hydrogels, and they are reviewed by Amsden and Li et al. (Amsden 1998; Metters 2006). These could be employed to estimate the diffusion coefficients of species in the synthesized gels. Diffusion of molecules is described by Fick's second law:

$$\frac{dC_A}{dt} = D\frac{d^2C_A}{dx^2}$$

This one-dimensional version of the law states that the rate of change of the concentration, C_A, is proportional to concentration profile in the x-direction by the diffusion coefficient D. Given initial conditions and a value for D, this equation can be solved to give the concentration as a function of space and time.

Several theories have tackled the challenge of finding D. Free volume theory imagines that solute diffuses through a polymer by jumping into voids temporarily created by thermal motion of the polymer and solvent. Mathematically, the diffusivity in the gel, D_g, is the diffusivity at infinite dilution, D_0, adjusted by the probability P_0 that the solute finds an opening between the polymer chains and a term expressing the likelihood of a free volume being created:

$$\frac{D_g}{D_0} = P_0 \exp\left(-\frac{Ba^*}{v_{f,w}}\left(\frac{\varphi}{1-\varphi}\right)\right)$$

B is a proportionality constant, a* is the cross section of the solute molecule, $v_{f,w}$ is the free volume per molecule of water, and is the volume fraction of polymer in the gel. Many functional forms of P_0 and variations of this formula have been proposed.

Hydrodynamic theory treats the solute as a sphere whose movement is impeded by frictional drag created by the no-slip boundary conditions at the stationary polymer strands. A model advanced by Cukier relates the frictional drag to the adjusted diffusivity as

$$\frac{D_e}{D_0} = \exp\left[-\left(\frac{3\pi L_c N_A}{M_f \ln(L_c/2r_f)}\right) r_s \varphi^{1/2}\right]$$

Where L_c is the length of the polymer chain, M_f is the molecular weight of the polymer, r_s is the radius of the solute, and r_f is the radius of the polymer.

Obstruction theories assume the diffusive path length is increased by impenetrable polymer strands. A model defines □ as the average radius of opening between straight randomly oriented polymer fibers and expresses the adjusted diffusivity as

$$\frac{D_g}{D_0} = \exp\left(-\frac{\pi}{4}\left(\frac{r_s + r_f}{\bar{r} + r_f}\right)^2\right)$$

Theoretically, movement of molecules into or out of hydrogels can be swelling controlled or diffusion controlled. Drug release from a swelling controlled system has been modeled with curve-fitting parameters for polymer relaxation and drug diffusion (Metters 2006). It has also

been modeled with simultaneous equations for diffusion and polymer dissolution with diffusion coefficients dependent on the degree of water influx (J. Siepmann 2002).

7. Conclusion

The goal of my research was to design and synthesize a SWNT/polymer-protein A complex to optically report antibody binding via a change in near infrared fluorescent emission. The idea behind the design was that the specificity of the sensor would be conferred by the naturally high affinity interaction between protein A and the Fc region of an antibody. However, the polymers used to suspend SWNT showed significant responses to antibodies in the absence of protein A and to generic proteins such as BSA. This is problematic because without a specific high affinity interaction of the SWNT construct with the antibody, and a minimal response to other molecules, it is difficult to envision how a single type of molecule could be recognized in a fermentation, which is a rich soup of lipids, sugars, proteins, and ions.

In the chitosan hydrogel system the time scale of the fluorescence responses are somewhat fast compared to the time scale for nickel to diffuse into the gel expected from literature. For protein A, EGFP, IgG of all the species tested, and BSA, the observed responses seem to be orders of magnitude faster than can be explained by diffusion of the proteins into the bulk of the gel. Responses at low concentrations of IgG also show that there is a response that cannot be due to IgG and Protein A binding. The observed responses may be due to interactions taking place at the interface of the gel and the solution. Alternatively, there may be large defects in the gel or there may be diffusion of a smaller species with higher mobility than the proteins, such as buffer ions or protons, which could change the water, chitosan, and ions participating in quenching SWNT photoluminescence.

Future research on constructing a SWNT/polymer-protein A sensor could proceed by searching for a polymer which wraps SWNT and prevents nonspecific interactions which modulate nanotube fluorescence. This would theoretically allow for a specific response only to antibody binding protein A, given that attachment of protein A onto the polymer is possible and that signal transduction takes place once the antibody binds to the protein A. A possible candidate,

not previously investigated by the Strano group, is Pluronic 103, which was shown to prevent nonspecific binding on SWNT by using a quartz crystal microbalance (Robert J. Chen 2003). Pluronics are triblock copolymers made of poly(ethylene oxide) and poly(propylene oxide) which are hypothesized to create a very hydrophilic, charge-neutral surface, which blocks nonspecific hydrophobic and electrostatic interactions.

More work toward understanding the mechanism of fluorescence response in the chitosan hydrogel would be interesting. Scanning electron microscopy images, or an alternative characterization of pore size, and work on immobilization of histagged EGFP exclusively in the presence of NTA/Ni would be particularly useful. Hydrogels provide an attractive way to immobilize SWNT in sensing applications, but solutes may alter the pH in the gel, ionic strength in the gel, or the overall gel swelling, which may have a complicating effect on SWNT fluorescence independent of more direct solute interaction with the SWNT. Sensors dependent on pH or ionic strength are unlikely to be useful with cell based systems, where these variables will be significantly affected by normal cell metabolism and not only the addition of a specific solute. However, they may still be useful in more controlled conditions.

8. Supplementary Matlab code

```
%chitosanHydrogelRealtimeGraph.m: outputs data like Figure 20 with points
%colored for addition and washing

%Set f,washframes,additionframes,and SECONDSPERFRAME before running

close all;


SECONDSPERFRAME=10;
washframes =[57 58 59];
additionframes = [25 26 87 88];
reads = zeros(1000,1);

for filenum=1:1000
    f = ['C:\Users\pbojo\Desktop\MEng\8211 chitosan chip\run9_',
num2str(filenum),'.txt'];
    try
        [wavelength r] = textread(f,'%f %f');
```

```
    catch
        break;
    end

    reads(filenum) = r(find(wavelength==996.238));
end
reads(filenum:end)=[];

nonwashreads = reads; nonwashreads(washframes) = [];
nonwashreadframes = 1: filenum-1; nonwashreadframes(washframes) =[];

washreads = reads(washframes);
additionreads = reads(additionframes);
plot(nonwashreadframes*SECONDSPERFRAME/60.0,nonwashreads,'o');
hold on;
plot(washframes*SECONDSPERFRAME/60.0,washreads,'go');
plot(additionframes*SECONDSPERFRAME/60.0, additionreads,'ro');

xlabel('Minutes'); ylabel('Intensity count');

%imageHistograms.m: outputs median fluorescence of an image
%set numrows,numcols before running

numrows = 5;
numcols = 4;

for row=1:numrows
    for col=1:numcols
        I = imread(['C:\Users\pbojo\Desktop\MEng\egfp
flourescence3\8_22_11_egfptestwithni\',num2str(row),'_',
num2str(col),'.tif']);
        fprintf('%d\n',median(median(I)));
    end
end


%equilibriumData.m: generates average flourescence quenching and standard
%deviation data, used for graphs such as Figure 12
close all;

%%%%%%%%%%%%%%%%VARIABLES TO SET BEFORE RUNNING SCRIPT
totalrows=3;
totalcols=4;
ratioindex=100;  %100 is 997nm.
%%%%%%%%%%%%%%%%

controlwavelength = zeros(totalrows*totalcols,512);
controlintensity = zeros(totalrows*totalcols,512);
wavelength = zeros(totalrows*totalcols,512);
intensity = zeros(totalrows*totalcols,512);

for rows=1:totalrows
    for cols=1:totalcols
          f =  ['C:\Users\pbojo\Desktop\MEng\cPVA SWNT ProteinA data\more
data control\',num2str(rows),'_',num2str(cols),'_1.txt']
```

```
          f2 =  ['C:\Users\pbojo\Desktop\MEng\cPVA SWNT ProteinA data\more
data 24hr after\',num2str(rows),'_',num2str(cols),'_1.txt']

        [controlwavelength(totalcols*(rows-1)+cols,:)
controlintensity(totalcols*(rows-1)+cols,:)] = textread(f,'%f %f');
        [       wavelength(totalcols*(rows-1)+cols,:)
intensity(totalcols*(rows-1)+cols,:)] = textread(f2,'%f %f');
    end
end

shifts=[];   %the percentage shifts after antibody addition
for rows=1:totalrows
    for cols=1:totalcols

       shifts(end+1)=((intensity(totalcols*(rows-1)+cols,ratioindex))-
controlintensity(totalcols*(rows-1)+cols,ratioindex))...
                /max(controlintensity(totalcols*(rows-
1)+cols,ratioindex))*100;
    end
end
%PRINT AVERAGE SHIFTS
for cols=1:totalcols
    indexes = cols:totalcols:totalcols*3;
    if size(indexes,2)==0
        break;
    end
      fprintf('%.1f%%\n',mean(shifts(indexes)));
end

%PRINT STANDARD DEVIATIONS (variance of error in control and sample
%measurement add)
fprintf('\nPrinting Standard deviations\n');
controlindexes = 1:totalcols:totalcols*3;
for cols=1:totalcols
    indexes = cols:totalcols:totalcols*3;
    if size(indexes,2)==0
        break;
    end
    fprintf('%.1f%%\n',sqrt( var(shifts(indexes))+var(shifts(controlindexes))
));
end
```

9. References

A. A. Shvedova, E. K., A. R. Murray, V. J. Johnson, O. Gorelik,S. Arepalli, A. F. Hubbs, R. R. Mercer, P. Keohavong, N. Sussman, J. Jin, J. Yin, S. Stone, B. T. Chen, G. Deye, A. Maynard, V. Castranova, P. A. Baron, and V. E. Kagan (2008). "Inhalation vs. aspiration of single-walled carbon nanotubes in C57BL/6 mice: inflammation, fibrosis, oxidative stress, and mutagenesis." American Journal of Physiology- Lung Physiology **295**(4): 552-565.

Al-Rubeai, S. M. B. a. M. (2007). "Selection methods for high-producing mammalian cell lines." Trends in Biotechnology **25**(9): 425-432.

Amroy (2011). Hybtonite Research Summary.

Amsden, B. (1998). "Solute Diffusion within Hydrogels. Mechanisms and Models." Macromolecules **31**: 8382-8395.

Ando, T. (2009). "The electronic properties of graphene and carbon nanotubes." Nature Asia Materials **1**(1): 17-21.

Ank Valstar, M. A., and Wyn Brown (2000). "The Interaction of Bovine Serum Albumin with Surfactants Studied by Light Scattering." Langmuir **16**(3): 922-927.

Anni J. Siitonen, D. A. T., Sergei M. Bachilo and R. Bruce Weisman (2010). "Surfactant-Dependent Exciton Mobility in Single-Walled Carbon Nanotubes Studied by Single-Molecule Reactions." Nano Letters **10**(5): 1595-1599.

Carter, A. C. C. P. J. (2010). "Therapeutic antibodies for autoimmunity and inflammation." Nature Reviews Immunology **10**: 301-316.

Catalent (2011). "GPEx Technology." from http://www.catalent.com/index.php/development/biologics/gpex.

Daniel A. Heller, S. B., Thomas E. Eurell, and Michael S. Strano (2005). "Single-Walled Carbon Nanotube Spectroscopy in Live Cells: Towards Long-Term Labels and Optical Sensors." Advanced Materials **17**: 2793-2799.

Enrico A Sturaa, M. G., Michael J Taussigb, Brian Suttonc, Michael G Gored, Gregg J Silvermane and Jean-Baptiste Charbonniera (2001). "Crystallization of macromolecular complexes: stoichiometric variation screening." Journal of Crystal Growth **232**(1): 580-590.

Faiella G, M. P., Di Florio G, Buosciolo A, D'Orazio L, Antonucci V, Giordano M (2009). "Monitoring the dispersion process of SWNTs in aqueous solutions by UV-vis and Raman spectroscopies." Journal of Nanoscience and Nanotechnology **9**(10): 6026-6033.

Farid, S. (2007). "Process economics of industrial monoclonal antibody manufacture." Journal of Chromatography B **848**: 8-18.

Fenno, J. (2007) mAb Manufacture: the Challenges Facing Small Companies. Innovations in Pharmaceutical Technology

Flygare, B. W. a. W. (1971). "The Simultaneous Measurement of the Electrophoretic Mobility and Diffusion Coefficient in Bovine Serum Albumin Solutions by Light Scattering." Chemical Physical Letters **12**(1): 81-85.

Gilbert L, T. J., Välilehto O, Saloniemi T, Cunningham C, White D, Mäkelä AR, Korhonen E, Vuento M, Oker-Blom C. (2006). "Truncated forms of viral VP2 proteins fused to EGFP assemble into fluorescent parvovirus-like particles." Journal of Nanobiotechnology **4**(13).

Guang Jia, H. W., Lei Yan, Xiang Wang, Rongjuan Pei, Tao Yan, Yuliang Zhao, and Xinbiao Guo (2009). "Cytotoxicity of Carbon Nanomaterials: Single-Wall Nanotube, Multi-Wall Nanotube, and Fullerene." Environmental Science & Technology **39**(5): 1378-1383.

Hamilton, R. (2001). The Human IgG Subclasses, Calbiochem.

Hamilton RG, R. C., Rodkey LS (1987). "Quality control of murine monoclonal antibodies using isoelectric focusing affinity immunoblot analysis." Hybridoma **6**(2): 205-217.

Hasemann CA, C. J. (1989). Fundamental immunology. New York, Raven Press.

Hober S, N. K., Linhult M (2007). "Protein A chromatography for antibody purification." Journal of Chromatography B **848**(1): 40-47.

Hong Jin, D. A. H., Marie Kalbacova, Jong-Ho Kim, Jingqing Zhang, Ardemis A. Boghossian, Narendra Maheshri and Michael S. Strano (2010). "Detection of single-molecule H2O2 signalling from epidermal growth factor receptor using fluorescent single-walled carbon nanotubes." Nature Nanotechnology **5**: 302-309.

Ida Genta, M. C., Annalia Astic, Bice Contia and Luisa Montanarib (1998). "Influence of glutaraldehyde on drug release and mucoadhesive propertiesnext term of chitosan previous termmicrospheres." Carbohydrate Polymers **36**(2): 81-88.

Ingemar Bjork, B.-A. P., John Sjoquist (1972). "Some Physicochemical Properties of Protein A from Staphylococcus aureus." European Journal of Biochemistry **29**: 579-584.

Initiative, G. a. B. (2010). "Technical challenges in defining mAbs."

J. Berger, M. R., J.M. Mayer, O. Felt, N.A. Peppas, R. Gurny (2004). "Structure and interactions in covalently and ionically crosslinked chitosan hydrogels for biomedical applications." European Journal of Pharmaceutics and Biopharmaceutics **57**: 19-34.

J. Siepmann, A. S., and N. A. Peppas (2002). "Understanding and Predicting Drug Delivery from Hydrophilic Matrix Tablets Using the "Sequential Layer" Model." Pharmaceutical Research **19**(3).

J.K. Armstrong , R. B. W., H.J. Meiselman and T.C. Fisher (2004). "The Hydrodynamic Radii of Macromolecules and Their Effect on Red Blood Cell Aggregation." Biophysical Journal **87**(6): 4259-4270.

James, S. D. a. D. (2009). Cell Line Development, Springer Science and Business Media.

Jeffrey L.Dangl, T. G. W., Sherie L.Morrison, Lubert Stryer, Leonard A.Herzenberg and Vernon T.Oi (1988). "Segmental flexibility and complement fixation of genetically engineered chimeric human, rabbit and mouse antibodies." The EMBO Journal **7**(7): 1989-1994.

Jin-Ho Ahn, J.-H. K., Nigel F. Reuel, Paul W. Barone, Ardemis A. Boghossian, Jingqing Zhang, Hyeonseok Yoon, Alice C. Chang, Andrew J. Hilmer, Michael S. Strano (2011). "Label-Free, Single Protein Detection on a Near-Infrared Fluorescent Single-Walled Carbon Nanotube/Protein Microarray Fabricated by Cell-Free Synthesis." Nano Letters(11): 2743-2752.

Jin Ji, J. G. O. C., David J. D. Carter, and Dale N. Larson (2008). "High-Throughput Nanohole Array Based System To Monitor Multiple Binding Events in Real Time." Analytical Chemistry **80**: 2491-2498.

Jonathan Brege, C. G., and Andrew Barron (2009). "Fluorescence Quenching of Single-Walled Carbon Nanotubes with Transition-Metal Ions." Journal of Physical Chemistry **113**: 4270-4276.

Jong-Ho Kim, J.-H. A., Paul W. Barone, Hong Jin, Jingqing Zhang, Daniel A. Heller, and Michael S. Strano (2010). "A Luciferase/Single-Walled Carbon Nanotube Conjugate for Near-Infrared Fluorescent Detection of Cellular ATP." Angew. Chem **49**: 1456 –1459.

Kerry Routenberg Love, V. P., Bo Jiang, Terrance A. Stadheim, J. Christopher Love (2010). "Integrated Single-Cell Analysis Shows Pichia pastoris Secretes Protein Stochastically." Biotechnology and Bioengineering **106**(2): 319-325.

Kling, J. (2009). "First US approval for a transgenic animal drug." Nature Biotechnology **27**(4).

Krajewska, B. (2001). "Diffusion of metal ions through gel chitosan membranes." Reactive & Functional Polymers **47**: 37-47.

L. R. Hirsch, R. J. S., J. A. Bankson, S. R. Sershen, B. Rivera, R. E. Price, J. D. Hazle, N. J. Halas, J. L. West (2003). "Nanoshell-mediated near-infrared thermal therapy of tumors under magnetic resonance guidance." PNAS **100**(23): 13549–13554.

Laurent Cognet, D. A. T., John-David R. Rocha, Condell D. Doyle, James M. Tour and R. Bruce Weisman (2007). "Stepwise Quenching of Exciton Fluorescence in Carbon Nanotubes by Single-Molecule Reactions." Science **316**(5830): 1465-1468.

Metters, C.-C. L. a. A. (2006). "Hydrogels in Controlled Release Formulations: Network Design and Mathematical Modeling." Advanced Drug Delivery Reviews **58**: 1379-1408.

Nano-C (2011). "Nanotubes." from http://www.nano-c.com/.

NanoTechnologies, S. (2011). "What is CoMoCat?". from http://www.swentnano.com/tech/what_is_comocat.php.

Nieba L, N.-A. S., Persson A, Hämäläinen M, Edebratt F, Hansson A, Lidholm J, Magnusson K, Karlsson AF, Plückthun A (1997). "BIACORE analysis of histidine-tagged proteins using a chelating NTA sensor chip." Analytical Biochemistry **252**(2): 217-228.

Olech, B. K. a. A. (1996). "Pore structure of gel chitosan membranes. I. Solute diffusion measurements." Polymer Gels and Nerworks **4**: 33-43.

Paul W. Barone, H. Y., Rene´ Ortiz-Garcı´a, Jingqing Zhang, Jin-Ho Ahn, Jong-Ho Kim, and Michael S. Strano (2009). "Modulation of Single-Walled Carbon Nanotube Photoluminescence by Hydrogel Swelling." ACS Nano **3**(12): 3869–3877.

Phillip Peterson, J. V., L Sabath and Paul Quie (1977). "Effect of Protein A on Staphylococcal Opsonization." Infection and Immunity **15**(3): 760-764.

Recht MI, D. B. D., Bell AG, Wolkin MV, Peeters E, Anderson GB, Kolatkar AR, Bern MW, Kuhn P, Bruce RH, Torres FE (2008). "Enthalpy array analysis of enzymatic and binding reactions." Analytical Biochemistry **377**(1): 33-39.

Robert J. Chen, S. B., Katerina A. Drouvalakis, Nadine Wong Shi Kam, Moonsub Shim, Yiming Li, Woong Kim, Paul J. Utz, and Hongjie Dai (2003). "Noncovalent functionalization of carbon nanotubes for highly specific electronic biosensors." PNAS **100**(9): 4984–4989.

Saito, R. D., M. S.; Dresselhaus, G. (1998). Physical Properties of Carbon Nanotubes. London, Imperial College Press.

Sandipan Ray, G. M. a. S. S. (2010). "Label-free detection techniques for protein microarrays: Prospects, merits and challenges." Proteomics **10**: 731-748.

Sang-Yong Ju, W. P. K. a. F. P. (2009). "Brightly Fluorescent Single-Walled Carbon Nanotubes via an Oxygen-Excluding Surfactant Organization." Science **323**(5919): 1319-1323.

Satishkumar, B., Gao, Wang, Wang, and Doorn (2007). "Reversible fluorescence quenching in carbon nanotubes for biomolecular sensing." Nature Nanotechnology **2**: 560-564.

ScienceDaily (2009). "Carbon Nanotubes Are Superior To Metals For Electronics, According to Engineers."

Steven Knecht, D. R., Alex N. Eberleb and Beat Ernst (2008). "Oligohis-tags: mechanisms of binding to Ni2R-NTA surfaces." Journal of Molecular Recognition **22**(4): 270-279.

Strano, J. H. C. a. M. S. (2007). "Solvatochromism in single-walled carbon nanotubes." Applied Physics Letters **90**.

Sudipto K. De, N. R. A., B. Johnson, W. C. Crone, David J. Beebe, and J. Moore (2002). "Equilibrium Swelling and Kinetics of pH-Responsive Hydrogels: Models, Experiments, and Simulations." Journal of Microelectromechanical Systems **11**(5): 544-555.

Thommes, A. S. a. J. (2010). "Recent advances in large-scale production of monoclonal antibodies and related proteins." Trends in Biotechnology **28**(5): 253-261.

Valerian E. Kagan, N. V. K., Weihong Feng, Brett L. Allen, Jennifer Conroy, Yuri Volkov, Irina I. Vlasova, Natalia A. Belikova, Naveena Yanamala, Alexander Kapralov, Yulia Y. Tyurina, Jingwen Shi, Elena R. Kisin, Ashley R. Murray, Jonathan Franks, Donna Stolz, Pingping Gou, Judith Klein-Seetharaman, Bengt Fadeel, Alexander Star & Anna A. Shvedova (2010). "Carbon nanotubes degraded by neutrophil myeloperoxidase induce less pulmonary inflammation." Nature Nanotechnology **5**: 354-359.

Walsh, G. (2010). "Biopharmaceutical benchmarks 2010." Nature Biotechnology **28**(9): 917-924.

Wang X, L. Q., Xie J, Jin Z, Wang J, Li Y, Jiang K, Fan S. (2009). "Fabrication of ultralong and electrically uniform single-walled carbon nanotubes on clean substrates." Nano Letters **9**(9): 3137-3141.

Warren Pilbrough, T. P. M., Peter Gray (2009). "Intraclonal Protein Expression Heterogeneity in Recombinant CHO Cells." PLoS One **4**(12).

Wayne U. Wang, C. C., Keng-hui Lin, Ying Fang, and Charles M. Lieber (2005). "Label-free detection of small-molecule–protein interactions by using nanowire nanosensors." PNAS **102**(9): 3208-3212.

Wells, A. B. a. J. (1996). "Minimizing a binding domain from protein A." PNAS **93**: 5688-5692.

Xiaoling Wang, T. K. D., Satish K. Singh and Sandeep Kumar (2009). "Potential aggregation prone regions in biotherapeutics." mAbs **1**(3): 254-267.

Y.Y. Fei, J. P. L., Y.S. Sun, J.T. Luo, X.B. Wang, K.S Lam, and X.D. Zhu (2008). "A novel high-throughput scanning microscope for label-free detection of protein and small-molecule chemical microarrays." Rev Sci Instruments **79**(1).

Ye, J., Alvin, K., Latif, H., Hsu, A., Parikh, V., Whitmer, T., Tellers, M., de la Cruz Edmonds, M. C., Ly, J., Salmon, P. and Markusen, J. F. (2010). "Rapid protein production using CHO stable transfection pools." Biotechnology Progress **26**(5): 1431-1437.

Yoon Jeong Park, Y. M. L., Si Nae Park, Seung Yoon Sheen, Chong Pyoung Chung and Seung Jin Lee (2000). "Platelet derived growth factor releasing chitosan sponge for periodontal bone regeneration." Biomaterials: 153-159.

Zhang, J. Q., A. A. Boghossian, et al. (2011). "Single Molecule Detection of Nitric Oxide Enabled by d(AT)(15) DNA Adsorbed to Near Infrared Fluorescent Single-Walled Carbon Nanotubes." Journal of the American Chemical Society **133**(3): 567-581.

Zhuang Liu, C. D., Weibo Cai, Lina He, Xiaoyuan Chen, and Hongjie Dai (2008). "Circulation and long-term fate of functionalized, biocompatible single-walled carbon nanotubes in mice probed by Raman spectroscopy." PNAS **105**(5): 1410–1415.